AD-A109 736 AERODYNE RESEARCH INC BEDFORD MA F/G 4/2
FALLING SNOW OPTICAL MODELING,(U)
NOV 81 M MARTINEZ-SANCHEZ, D S DVORE DAAD07-81-C-0009
UNCLASSIFIED ERADCOM/ASL-CR-81-0009-1 NL

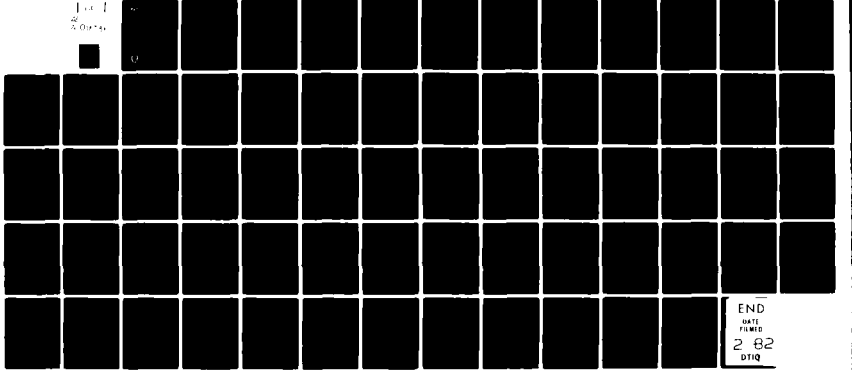

END
DATE FILMED
2-82
DTIC

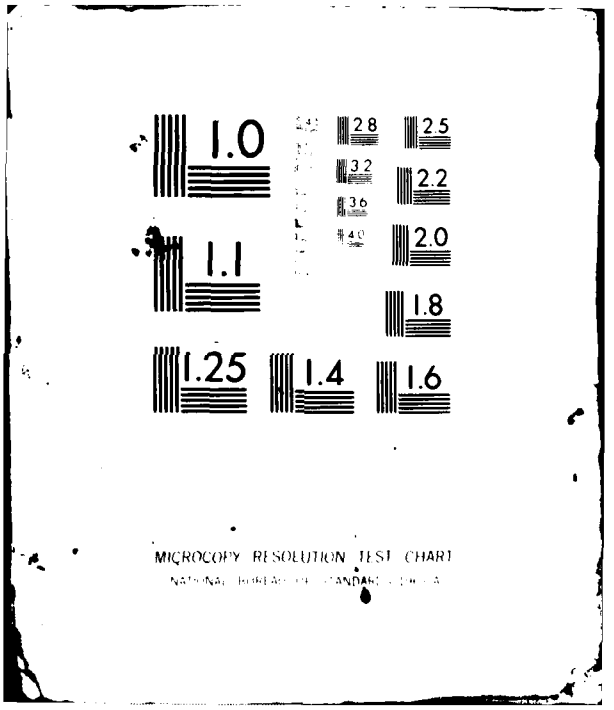
1.0
1.1
1.25
1.4
1.6
1.8
2.0
2.2
2.5
2.8
3.2
3.6
4.0
MICROCOPY RESOLUTION TEST CHART

-CR-81-0009-1

AD
Reports Control Symbol
OSD - 1366

13

LEVEL II

FALLING SNOW OPTICAL MODELING

NOVEMBER 1981

By

Manuel Martinez-Sanchez
David S. Dvore
John F. Ebersole
Roberto Vaglio-Laurin
Thomas E. Spaulding

Aerodyne Research, Inc.
Bedford Research Park, Crosby Drive
Bedford, MA 01730

UNDER CONTRACT: DAAD07-81-C-0009

CONTRACT MONITOR: Mary Ann Seagraves

Approved for public release; distribution unlimited.

US Army Electronics Research and Development Command
Atmospheric Sciences Laboratory
White Sands Missile Range, NM 88002

NOTICES

Disclaimers

The findings in this report are not to be construed as an official Department of the Army position, unless so designated by other authorized documents.

The citation of trade names and names of manufacturers in this report is not to be construed as official Government indorsement or approval of commercial products or services referenced herein.

Disposition

Destroy this report when it is no longer needed. Do not return it to the originator.

SECURITY CLASSIFICATION OF THIS PAGE (When Data Entered)

REPORT DOCUMENTATION PAGE		READ INSTRUCTIONS BEFORE COMPLETING FORM
1. REPORT NUMBER ASL-CR-81-0009-1	2. GOVT ACCESSION NO. AD-A109 736	3. RECIPIENT'S CATALOG NUMBER
4. TITLE (and Subtitle) FALLING SNOW OPTICAL MODELING		5. TYPE OF REPORT & PERIOD COVERED Contractor Report 6. PERFORMING ORG. REPORT NUMBER
7. AUTHOR(s) Manuel Martinez-Sanchez, David S. Dvore, John F. Ebersole, Roberto Vaglio-Laurin, Thomas E. Spaulding		8. CONTRACT OR GRANT NUMBER(s) DAAD07-81-C-0009
9. PERFORMING ORGANIZATION NAME AND ADDRESS Aerodyne Research, Inc. Crosby Drive Bedford, MA 01730		10. PROGRAM ELEMENT, PROJECT, TASK AREA & WORK UNIT NUMBERS
11. CONTROLLING OFFICE NAME AND ADDRESS US Army Electronics Research and Development Command Adelphi, MD 20783		12. REPORT DATE NOVEMBER 1981 13. NUMBER OF PAGES 65
14. MONITORING AGENCY NAME & ADDRESS(if different from Controlling Office) US Army Atmospheric Sciences Laboratory White Sands Missile Range, NM 88002		15. SECURITY CLASS. (of this report) UNCLASSIFIED 15a. DECLASSIFICATION/DOWNGRADING SCHEDULE

16. DISTRIBUTION STATEMENT (of this Report)

Approved for public release; distribution unlimited

17. DISTRIBUTION STATEMENT (of the abstract entered in Block 20, if different from Report)

18. SUPPLEMENTARY NOTES

Contract Monitor: Mary Ann Seagraves

19. KEY WORDS (Continue on reverse side if necessary and identify by block number)

Snow	Snowfall	Visible	Condensation
Falling snow	Ice	Infrared	Accretion
Snowflake	Cloud	Transmission	
Snowstorm	Ice crystal	Extinction	

20. ABSTRACT (Continue on reverse side if necessary and identify by block number)

In order to develop a model describing the adverse weather effects of snow on optical transmission, it is necessary to incorporate optical, physical, and meteorological characteristics. We report on the development of a model which incorporates these three aspects of snow characterization. We first discuss a numerical model aimed at obtaining an understanding of the meteorological aspects of snowfall. Specifically, the model accepts as inputs such measurable quantities as temperature and dew point vertical profiles, as well as other quantities, often not measured, such as updraft velocity, cloud

DD FORM 1 JAN 73 1473 EDITION OF 1 NOV 65 IS OBSOLETE

390412

SECURITY CLASSIFICATION OF THIS PAGE (When Data Entered)

20. ABSTRACT (cont)

droplet size, and ice nucleus concentration. Based on these data, the model then predicts the time evolution of the cloud, and, eventually, the rate of precipitation and the type of snow particles arriving at the ground. We also discuss optical considerations in order to provide a framework in which physical and meteorological aspects can be included. Specifically, we discuss the need for areal, volume, and settling velocity parameters in calculating optical extinction coefficients.

ACKNOWLEDGEMENTS

This contract was monitored by Mary Ann Seagraves of the US Army Atmospheric Sciences Laboratory. Important technical contributions made by her to the program described in this report are gratefully acknowledged.

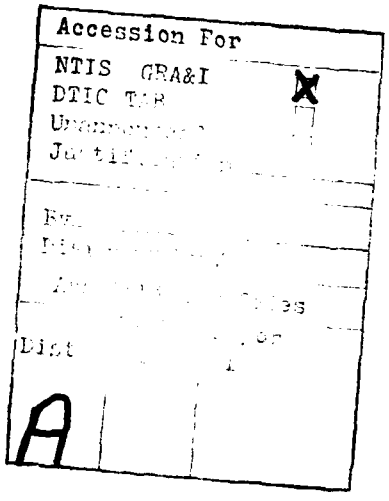

CONTENTS

LIST OF FIGURES

1. INTRODUCTION AND OVERVIEW

The clarification of the complex physical phenomena occurring in a snowstorm is of great interest, both scientifically and from a practical point of view. On the one hand, most of the snow cloud microphysics is repeated in the upper levels of a raincloud, and is therefore of very general meteorological interest. On the other hand, the strong impact of falling snow on visibility and transmission of various types of radiation, and the variability of these effects depending on intensity and type of snow[1] indicate the need for some understanding of the underlying mechanisms. In order to develop a falling snow model describing the adverse weather effects of snow on transmission, it is necessary to incorporate optical, physical, and meterological characteristics. We report on development of a model which incorporates these aspects of snow characterization.

In Sections 2 to 5, we report on the development of a numerical model of snowfall aimed at obtaining such an understanding. Specifically, the model accepts as inputs such measurable quantities as temperature and dew point vertical profiles, as well as other quantities, often not measured, such as updraft velocity, cloud droplet size and ice nucleus concentration. Based on these data, the model then predicts the time evolution of the cloud, and, eventually, the rate of precipitation and the type of snow particles arriving at the ground. This then provides some degree of closure, by allowing comparisons to such readily observable quantities as equivalent water precipitation rate and particle flux at the ground.

The model can display the sensitivity of the snowstorm to specific changes in the data, and can, therefore, serve as a guide in the analysis of test data, a check on hypotheses, and hopefully a way to generate simple rules and generalizations. It must be recognized that (a) the extent of the input

data that are known a priori is limited, since several key parameters are usually not measured, and (b) the details of some of the important mechanisms are not yet well enough understood to allow confident predictions. Given these limitations, one cannot hope to construct a truly predictive code.

We discuss in Section 6 optical considerations in order to provide a framework in which the results of the physical and meteorological modeling can eventually be linked to effects on transmission. Specifically, we discuss the need for area, volume, and settling velocity parameters in calculating optical extinction coefficients.

2. MODEL ASSUMPTIONS

Ice particles introduced in a supercooled water cloud can grow rapidly by vapor diffusion at the expense of evaporation from the liquid water. This mechanism, first postulated by Findeisen, is fundamental for initiating precipitation, particularly in the wintertime. It is due to the fact that the vapor pressure of liquid water exceeds that of ice by as much as 0.2 mm Hg for a range of temperatures below 0°C, the difference peaking at -12°C.

The ice growth rate will peak at ambient temperatures slightly below the peak of the differential vapor pressure curve (since the release of latent heat will slightly warm up the ice particle), and will be slower on either side of this maximum. This growth rate in turn determines the shape and type of ice crystals formed, and is the basis for ice habit diagrams such as that of Nakaya[2] or Magono and Lee[3] (1966). For instance, very slow growth (either near 0°C or below -25°C) will favor the thermodynamically stable equilibrium crystal habit, short columns, while fast growth gives prominence to kinetic effects which tend to accelerate growth of the prismatic faces and results in plate or branched plate formation between -10 and -20°C. The degree of ambient moisture has a secondary effect in affecting this habit selection. Thus, rules can be implemented in a model to select the correct crystal habit depending on local growth rate.

For a 1 km thick cloud the temperature difference between top and bottom is between 5 and 10°C, which is a relatively narrow range in a crystal habit diagram. Thus, we adopt the simplifying assumption that only one crystal type exists in the cloud. The type (plate, needle, or spherical) is selected a

priori, based on the given vertical profiles. Within each basic type, the degree of riming by supercooled drops is calculated in detail, and it results in a continuum of particle aspect ratios, leading, for heavy rime, to spherical graupel.

The origin of the ice crystals is one point of difficulty, since the state of knowledge is still imperfect and several mechanisms are involved (seeding from an overlying "seeder cloud", as originally proposed by Bergeron, or intra-cloud ice nucleation by contact or other mechanisms). In any case, ice nuclei appear preferentially at the cloud top. For modeling purposes, we bypass this difficult by treating the nuclei flux at cloud top in a parametric fashion.

One other element of modeling difficulty concerns the magnitude and distribution of the in-cloud updraft. For stratiform or nimbus types of clouds, this updraft is likely to be in the range of 0.1 to 0.5 m/s only, but since the fall speed of ice and snow particles is in that range as well, its influence is essential. Data on stratus cloud updraft are very scanty, and the planned SNOW tests do not comtemplate its measurement. Therefore, we treat this effect parametrically as well, and will have to rely on detailed comparison of model results with those data which <u>will</u> be available (lapse rate, dew point profile, synoptic weather data, ground precipitation data) in order to construct rules for selecting the proper updraft values.

We consider in the model a monodisperse water drop population. The effect of polydispersity of liquid water droplets on their accretion on ice particles was studied by Ryan[4]. While for the wide spectrum of a maritime cumulus cloud, there was a factor of 2 less growth if the mean size only was considered, the effect was negligible for a more concentrated continental cloud spectrum.

Most of our calculations are done using the assumption of no external air entrainment and mixing, although a mixing length parameter is specified and a sink term due to mixing is included in several of the equations (see below). Aside from this, the concentration of liquid water present is determined by an overall water balance that includes advection of vapor and condensation on ice particles. The latter is treated in a fully kinetic manner, but the growth of individual liquid droplets occurs over such short time scale that its inclusion as a kinetic equation would make the system of equations very stiff. Accordingly, above a threshold of 10^{-5} Kg/m^3 liquid water contents it is assumed that vapor-water equilibrium is maintained. In the presence of large enough ice concentrations, or if the supply of condensible vapor is weak for the available ice, the pressure of vapor may fall below water saturation; this is detected in the model by a tendency of the liquid water density, as calculated under the water equilibrium assumption, to drop. When the 10^{-5} Kg/m^3 threshold is crossed, the assumption of vapor-water saturation is abandoned. The drops are assumed to evaporate rapidly (in one time step) and the vapor concentration is then determined by the water balance equation, without a liquid term in it. The equation that controls the number density of water drops is, however, retained, so that the nuclei at least are assumed to remain present; if the vapor conservation equation indicates later a tendency to overshoot the water saturation level, re-nucleation is considered to occur, and the excess vapor is distributed over the water condensation nuclei.

Although the above procedure constitutes a satisfactory determination of the liquid water contents, the particle size has to be left as a model parameter. What is actually done is to specify at the cloud bottom the concentration of cloud condensation nuclei. This serves as the lower boundary condition for a droplet number conservation equation; the equaton itself accounts for time variation, convection in an inhomogeneous cloud, and loss of

drops due to accretion on ice. The droplet size then follows at each time and place from the water contents and the number density.

Accretion (riming) is modeled as a process of capture of droplets by the faster falling ice crystals. The capture efficiency depends quite critically on both, drop and crystal size; we use curve fits to the calculated efficiences of Refs. 5 and 6.

The accreted water is assumed to freeze on contact. This may not be true at high accretion rates and moderately warm temperatures, and some of the unfrozen water may then be shed off; however, the details of this are not very well understood, and for the present we ignore shedding. Formation of ice splinters upon accretion is also ignored, as is crystal breakage by the collision. The former is rarely observed for droplets smaller than 50 μm diameter, while the latter requires the presence of rather large drops (diameter > 250 μm). Thus, for the range of most interest in winter clouds (less than 50 μm diameter), ice multiplication processes can be at least tentatively neglected. The accreted mass is assumed to be added to the shorter particle dimension, until it becomes a spherical graupel particle. The density of accreting particles is at present taken to be 0.5 g/cm^3, but a more detailed model is probably needed.

The primary particle variable is its mass. Once this is known, well established dimensional relationships can be employed to infer the geometrical ratios for each type of particle, as well as its density. The prototype of these relationships for diffusional growth is the Auer-Veal rules, as complied for instance by Davis[7]. Densities are calculated according to Heymsfeld[8]. When both accretion and vapor growth are present, the particle diameter is assumed to grow purely due to the vapor deposition, at a rate determined by the rate of vapor condensation in the same manner as if no accretion existed. The accreted mass, on the other hand contributes to increase the thickness

only, as indicated. This procedure was also used, for example, by Young (Ref.9).

One final important assumption is at present made in the model, namely, ice particle agglomeration is neglected. This is consistent with our use of a single ice particle type and size, since ice-ice agglomeration is driven mostly by the difference of settling velocities. The adequacy of this criterion can be tested by comparing the ice-ice mean collision frequency to the inverse of the residence time for a particle; the criterion for no agglomeration is then found as

$$n_i < \frac{\bar{v}_i}{\Delta\bar{v}_i} \frac{1}{H A_i} \quad , \tag{1}$$

where n_i is the ice particle number density, $\bar{v}_i$ its mean fall velocity, with characteristic spread $\overline{\Delta v_i}$, A_i the particle frontal area and H the height of the cloud top. Assuming a power law $v_i = k\, a^b$ for the fall speed (where a = particle radius and b ≈ 0.3-0.6), we have $(\bar{\Delta}\ \overline{v_i})/\bar{v}_i = b\ (\bar{\Delta}\ \bar{a})/a$. For H = 2000m, a = 500 μm, b = 0.5 and $\bar{\Delta}\ \bar{a} \sim \bar{a}$ (as in an exponential distribution), the criterion for no agglomeration gives

$$n_i < 1.3 \times 10^3\ m^{-3} = 1.3\ (\text{liter})^{-1} \tag{2}$$

This density is exceeded in glaciated clouds (where however, a is probably smaller than 500 μm) or in thin layers of high concentration. Therefore, for clouds topping at less than about 2-3 km, agglomeration is not a dominant issue; it is even less so if only the in-cloud part of the ice crystal growth is of interest. As an example, the detailed set of data of

Ref. 10 show no agglomeration in clouds topping at about 2000m, even when the glaciated cloud top reaches ice concentrations of 20-40 $(\text{liter})^{-1}$.

However, this does not mean that conditions do not arise where agglomeration is important. Cloud top heights of over 3 km are not uncommon, and are, in fact, characteristic of the most intense snowstorms. In fact, our preliminary analysis of the data of the SNOW I test series[11] indicates the predominance of agglomeration effects (a discussion of these data appear elsewhere in the paper). Therefore, an extension of the model to cover such cases is very desirable from a practical viewpoint.

3. FORMULATION

The model consists of six one-dimensional, time-dependent partial differential equations for the following variables: ice particle number density (n_i), and mass (m_i), accreted mass per ice particle (m_a), ice particle major radius (a), droplet number density (n_d) and droplet mass (m_d). If mixing with outer air is neglected (case of very extensive stratus layers), the equations are:

$$\frac{\partial n_i}{\partial t} + \frac{\partial}{\partial y} (n_i v_i) = 0 \tag{3}$$

$$\frac{\partial n_d}{\partial t} + \frac{\partial}{\partial y} (n_d v_d) = - \frac{n_i}{m_d} \left(\frac{dm_i}{dt}\right)_{accr.} \tag{4}$$

$$\frac{\partial m_i}{\partial t} + v_i \frac{\partial m_i}{\partial t} = \left(\frac{dm_i}{dt}\right)_{\substack{vapor \\ diff.}} + \left(\frac{dm_i}{dt}\right)_{accr.} \tag{5}$$

$$n_d \left(\frac{\partial m_d}{\partial t} + v_d \frac{\partial m_d}{\partial y}\right) = -n_i \left(\frac{dm_i}{dt}\right)_{\substack{vapor \\ diff.}} - \frac{\partial \rho_v}{\partial t} - \frac{\partial}{\partial y} (\rho_v v_a) \tag{6}$$

$$\frac{\partial m_a}{\partial t} + v_i \frac{\partial m_a}{\partial y} = \left(\frac{\partial m_i}{dt}\right)_{accr.} \tag{7}$$

$$\frac{\partial a}{\partial t} + v_i \frac{\partial a}{\partial y} = \frac{(dm_i/dt)_{diff}}{(dm_i/da)_{diff}} \tag{8}$$

Here v_i and v_d are the net (upwards) velocity of ice particles and droplets respectively:

$$v_i = v_a - v_{i,\,settl} \tag{9}$$

$$v_d = v_a - v_{d,\,settl} \tag{10}$$

where V_a is the prescribed updraft velocity, and $v_{i,settl}$, $v_{d,settl}$ are the ice and droplet settling velocities, respectively. The vapor density ρ_v is taken as the water-equilibrium density (from a curve fit to the Clausius-Clapeyron equation) whenever $n_d m_d > 10^{-5}$ Kg/m^3. Since ρ_v then depends only on the ambient temperature (whose profile is prescribed), Eq. (6) can be viewed as governing the droplet mass m_d. On the other hand, if $n_d m_d < 10^{-5}$ Kg/m^3, m_d is set equal to zero, and Eq. (6) is turned around to become a conservation law for ρ_v (breaking the connection of ρ_v to T).

The diffusive rate of growth of ice particles is given by

$$\left(\frac{dm_i}{dt}\right)_{diff} = \frac{(C/\varepsilon_o)\, S_{v,i}}{\frac{RT_a}{e_{sat,i}(T_a) D_v' M_w} + \frac{L_s}{K_a' T_a}\left(\frac{L_s M_w}{R T_a} - 1\right)} \tag{11}$$

where C is the electrostatic capacitance of the particle (a function of its size and shape), $\varepsilon_o = 8.85 \times 10^{-12}$ in MKS units is the permittivity of free space, $S_{v,i}$ is the supersaturation relative to ice, R=8.314 Joule/(Mole °K) is the gas constant, $e_{sat,i}$ is the ice saturation vapor pressure, M_w is the molecular weight of water, L_s the heat of ice sublimation and D_v', K_a' are effective vapor diffusivity and air thermal conductivity, respectively. These effective transport properties incorporate correction factors for both free-molecular flow effects and high Reynolds number effects; details can be found for example in Ref. (12), Ch. 13. Equation (11) accounts in its formulation for the reduction of condensation rate due to particle heating by the release of latent heat. The ice supersaturation $S_{v,i}$ is calculated by

$$S = \frac{e_\infty}{e_{sat,i}(T_a)} - 1 \tag{12}$$

where

$$e_\infty = \rho_v R_v T \tag{13}$$

and e stands for the prevailing pressure of vapor ($e_\infty < e_{sat,w}(T_a)$).

Accretion growth for plate-like particles is given by:

$$\left(\frac{dm_i}{dt}\right)_{accr.} = E_c \pi (a_d + a_i)^2 \left(V_{FALL_i} - V_{FALL_d}\right) W_\ell \qquad (14)$$

where E_c is the collection efficiency,[5,6] a_d and a_i are the drop and plate radii, respectively, and W_ℓ is the local water content of the cloud. Similar expressions are used for other particle shapes.

Particle and droplet fall velocities are calculated using standard literature values of the drag coefficient for the various shapes and sizes. The calculation takes the form

$$N_{Re} = f\,(C_D N_{Re}^2) \qquad (15)$$

where

$$C_D N_{Re}^2 = \frac{8 m_i \rho_a g}{\pi \mu_a^2} \qquad (16)$$

can be calculated directly in terms of the particle mass m_i, f is a known function, depending on geometry only, and

$$N_{Re} = \frac{\rho_a V_{FALL} d}{\mu_a} \qquad (17)$$

is the particle Reynolds number, from which the fall velocity follows. Functions f for both oblate and prolate spheroids (as well as for spheres) have been incorporated in the model.

Equation (8) expresses the assumption that only vapor condensation can increase the particle major dimension, a. The quantity $(dm_i/da)_{diff}$ is calculated from the expressions in Refs. 7 and 8. For plates (in MKS units).

$$\left(\frac{dm_i}{da}\right)_{diff} = \begin{cases} 1.0123\ a^{1.475} & a < 1.6166\times10^{-4}\text{m} \\ 0.31925\ a^{1.098} & a > 1.6166\times10^{-4}\text{m} \end{cases} \qquad (18)$$

Mixing with external air is accounted for through a simple device. It is assumed that mixing is proportional to updraft strength v_a, inversely proportional to cloud horizontal extent, and proportional to the difference in densities of the mixing quantities (ice, water, and vapor densities). No enthalopy mixing is explicitly included, since the temperature profile is directly an input to the model. Introducing a "mixing length" ℓ_m (of the order of 5 times the horizontal radius of the cloud, according to Ref. 13), the additional terms on the right-hand sides of Eqs. (3),(4), and (6) are respectively

$$-\frac{v_a}{\ell_m}\ n_i \qquad (3a)$$

$$-\frac{v_a}{\ell_m}\ n_d \qquad (4a)$$

$$-\frac{v_a}{\ell_m}\ (\rho_v - \rho_{v,out}) \qquad (6a)$$

It can be seen by comparison of these terms with the convective derivative terms in the corresponding equations that mixing effects become significant only for clouds with thickness comparable to their diameter; for

extensive stratus (ℓ_m >> cloud thickness), mixing is only significant near the cloud edges.

The "natural" boundary conditions of the problem are: ice flux or ice number density and ice particle mass at cloud top, water droplet number density and zero droplet diameter at cloud base, zero accreted mass and prescribed particle diameter at cloud top, and water-saturation vapor density at cloud base.

In addition, the numerical procedure requires the remaining boundary conditions to be specified as well (on ice mass, diameter and accretted mass at cloud base, droplet density and diameter and vapor density at cloud top). We choose zero flux gradient conditions for these quantities, indicative of the fact that no changes (or only very slow ones) are expected outside the cloud.

The initial conditions are normally chosen to correspond to an ice-free supercooled cloud in a nonprecipitating steady state. Some inconsistency is incurred in that precipitation would be required to balance the vapor advection by the updraft, which is assumed constant in time. This initial inconsistency disappears gradually as ice phase precipitation develops from the cloud top down.

The system of partial differential equations is solved in time and space by the McCormick time-split method, accurate to first order in time and to second order in space. Typical mesh sizes are 20m and 5 sec (if droplet growth were modeled kinetically, a much shorter time step would be required). A slow growing numerical instability of short wavelength (two grid spaces) is noticed for some conditions. A periodic smoothing of the profiles using a local filter has been found to correct this problem.

4. APPLICATIONS OF THE MODEL

We present in this section some examples of the sort of results obtainable with the model just described. Although comparison to data is made difficult by the lack of detailed space-time measurements of in-cloud developments, some qualitative comparisons will be made to the data of Ref. 10. as well as (in the following section) to SNOW I test data.

Figures 4 through 7 present in detail the calculated time history of a snowstorm where most of the effects included in the model can be observed. The input data are as follows:

Cloud thickness: From 1000 to 2000m in altitude
Temperature profile: Linearly decreasing from -11°C to -17°C (8°C/km). This is close to moist adiabatic conditions.
Updraft: 17cm/sec, tapering to 8.5 cm/sec in the last 60m.
Ice nuclei flux: $1000/(m^2 sec)$ at cloud top
Ice nuclei size: 200 μ radius at cloud top
Droplet density: 2×10^8 m^{-3} at cloud base
Mixing length: 3000m
Ice particle type: plates (consistent with growth at about -15°C)

Some of these data were selected to match the conditions reported in Ref. 10 (temperatures, altitudes, droplet size, crystal type). In that work, clouds in different stages of development were observed during a two day period and in-cloud data were sampled (ice and water contents, crystal concentration and type). Although the clouds are classified as "incipient",

"mature" or "decaying", no information can be obtained regarding their earlier history or other conditions (updraft, nuclei flux).

Figure 1 shows the development of the ice density profile. After 1000 s from ice seeding initiation, the ice has penetrated some 800m into the cloud; accounting for the updrafts, this represents a settling velocity of some 95 cm/sec, which is typical of rimed sub-millimeter plates. The development from this time on is quite regular, with a gradual increase in ice concentration, approaching about 3 particles/liter. This increase indicates accumulation due to slower fall velocities as time increases; we will later trace it to the gradual disappearance of rime on the particles, as the cloud glaciates.

Figure 2 shows the development of ice crystal radius. The gradual increase with time corresponds also to the slower fall velocity, which gives each particle more residence time, and allows more growth by vapor diffusion. By about 11,000 sec, an acceleration of this growth is discernible; this can be correlated with the accumulation of crystals at cloud top, visible in Fig. 1 at 11,000 sec, and, as will be seen later, with the arrival of glaciation there. The disappearance of accretion leads to this local accumulation due to the very slow fall of the small ice crystals present at the top.

Figure 3 shows the accreted mass per particle. The main accretion event occurs between 1000 and 3000 sec, and the 1000 s profile shows a significant amount of riming; at the peak of this profile, about two thirds of a particle mass is in the accreted droplets. As time progresses, the accreted mass gradually disappears, and is insignificant at 11,000 sec.

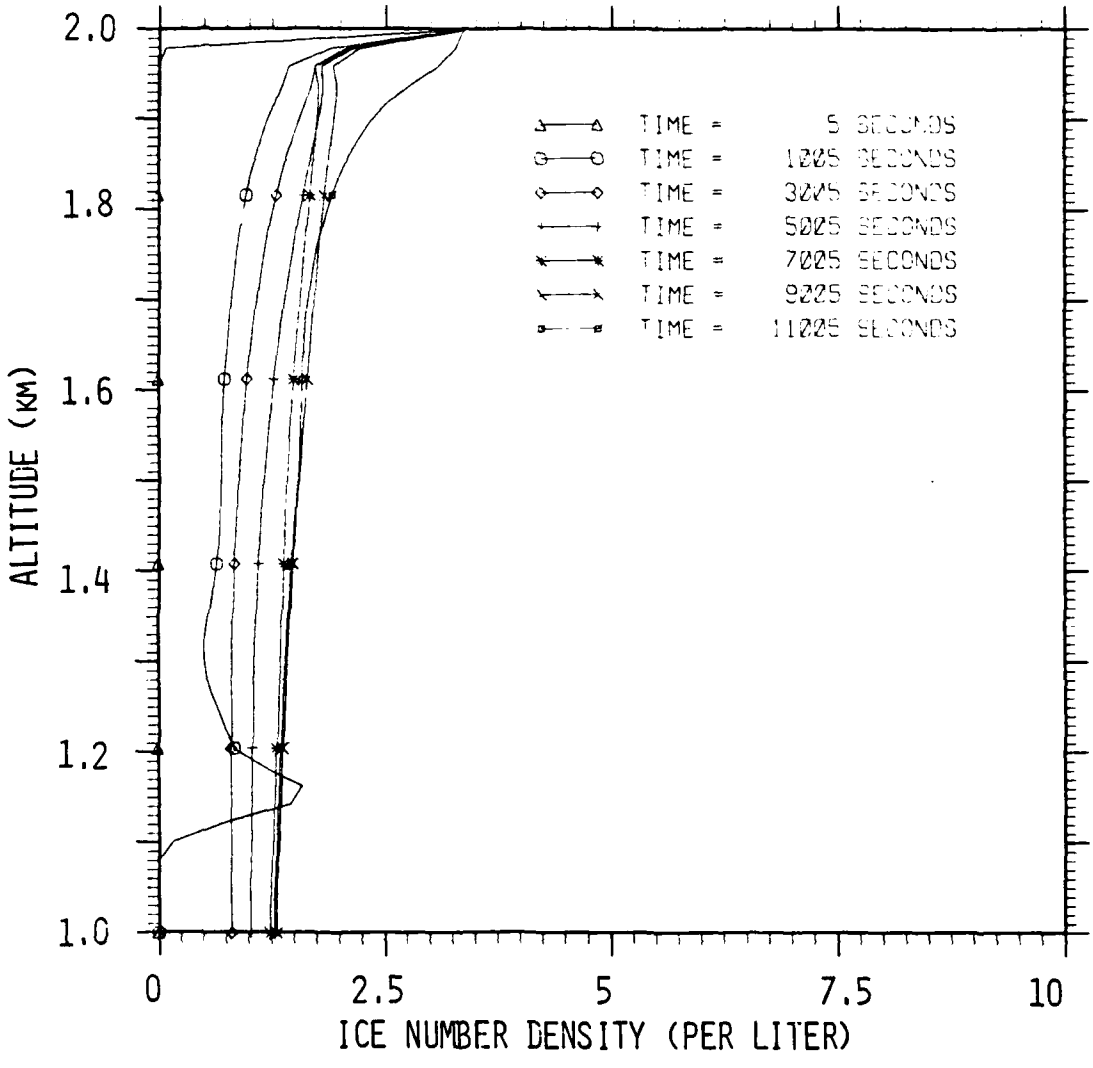

Fig. 1 - Ice Number Density, Ice Particle Flux at Cloud Top is 1000 $m^{-2}s^{-1}$, Water Droplet Density at Cloud Bottom is 200 cm^{-3}.

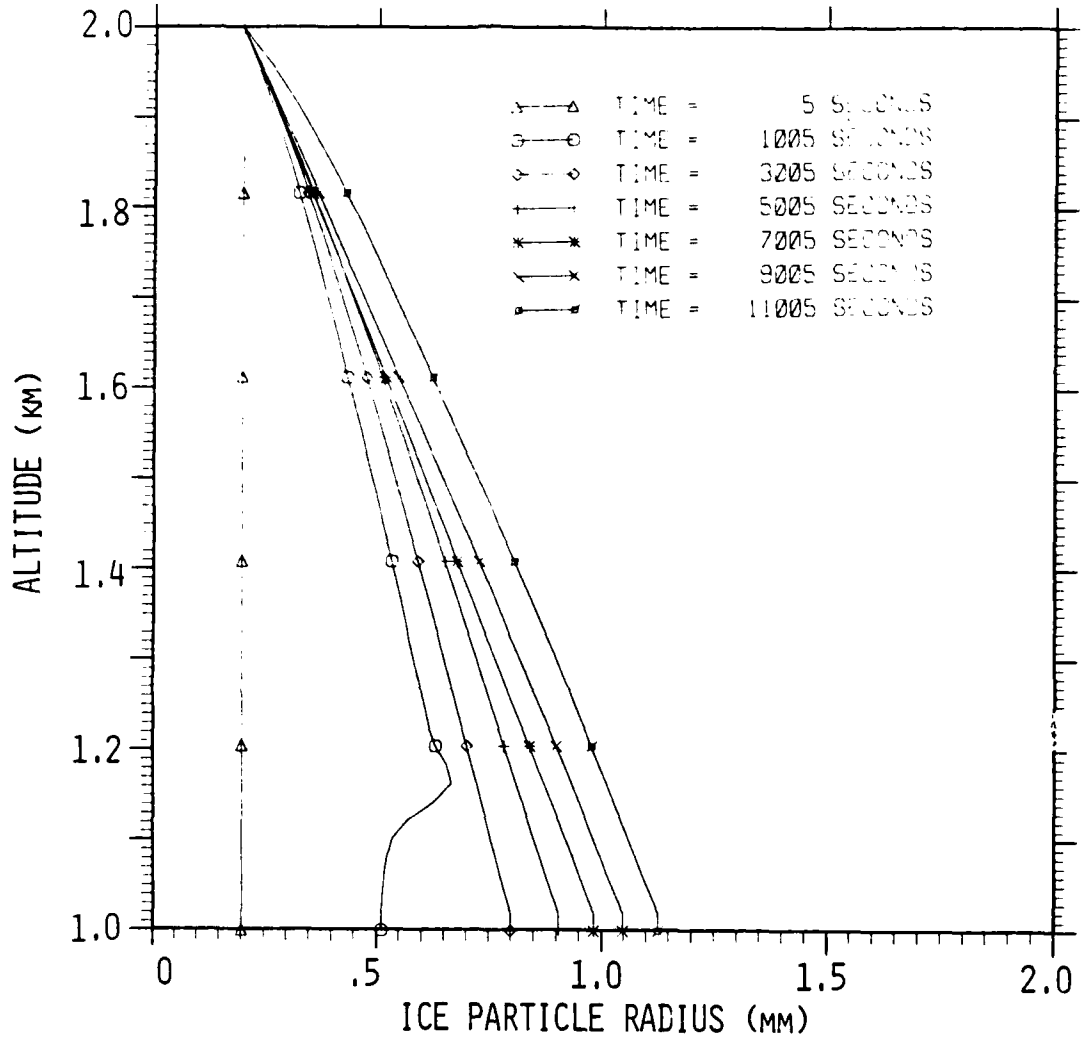

Fig. 2 - Ice Particle Radius. Ice Particle Flux at Cloud Top is 1000 $m^{-2}s^{-1}$, Water Droplet Density at Cloud Bottom is 200 cm^{-3}

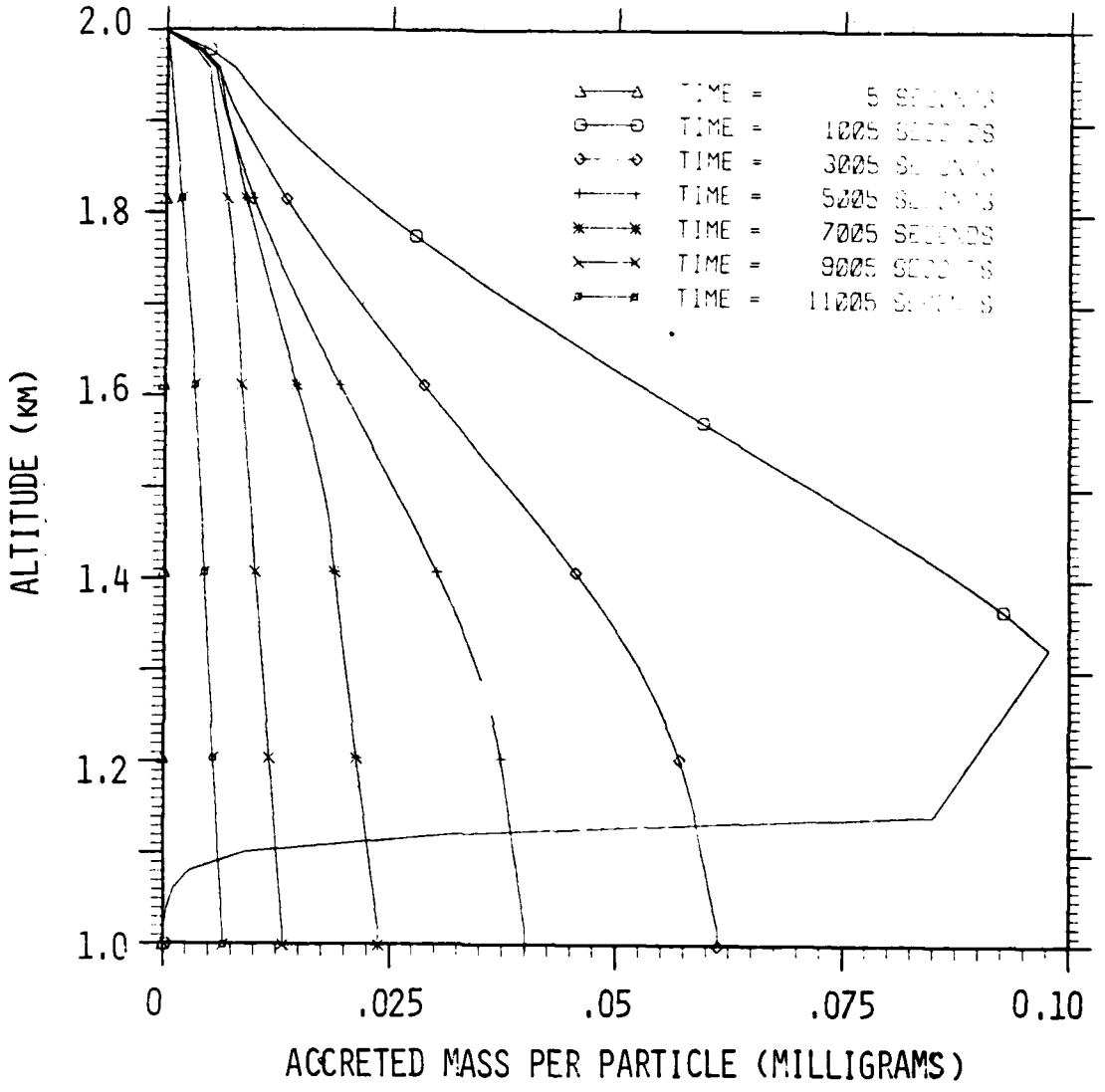

Fig. 3 - Accreted Mass per Particle. Ice Particle Flux at Top is 1000 $m^{-2}s^{-1}$. Water Droplet Density at Cloud Bottom is 200 cm^{-3}

The corresponding developments regarding the liquid phase are presented in Figs. 4, 5 and 6. In Fig. 4 we can observe the strong depletion of water droplets by the process of riming at t ≈ 3000-5000 sec, particularly in the upper third of the cloud, where the drops have diameters of about 20 μm, and are at the peak of their accretion efficiency. The reduction of their efficiency down the cloud, as the droplets become smaller (see Fig. 5) can be easily traced; it overcomes a partially compensatory effect associated with the higher capture efficiency of the growing ice crystals. As glaciation proceeds by evaporation of the droplets, the number density profile recovers to its original level, although by now it represents merely "dried out" nuclei. Figure 5 shows the slow progress of glaciation. The droplets first evaporate at cloud base, where the most ice surface is available; however, this is sensitive to parameters such as lapse rate and, possibly, agglomeration (not treated in the model). The survival of liquid water at cloud top is an artifact of the model, due to fictitious accumulation as the updraft tapers off. Of course, lateral divergence must exist, to compensate for this slowdown, and this should introduce an equivalent one-dimensional "sink" in the conservation equations. The total liquid water contents of the cloud is shown in Fig. 6, where a progression from a profile that reaches ≈ 1 g/m^3 at cloud top to essentially zero, can be seen to occur.

The vapor density is, of course, a driving factor throughout these developments. Its evolution is seen in Fig. 7. The initial profile is simply a reflection of the temperature profile assumed, since water saturation exists initially. At the latter times, when the cloud is glaciated, the vapor density falls very slightly below water saturation. A lower bound would probably exist at the ice saturation level (85-90% of water saturation at these temperatures), but this limit is not even approached; this means enough supersaturation still exists relative to the ice phase to ensure continued growth (see Fig. 2) in these later stages. In turn, this prevents

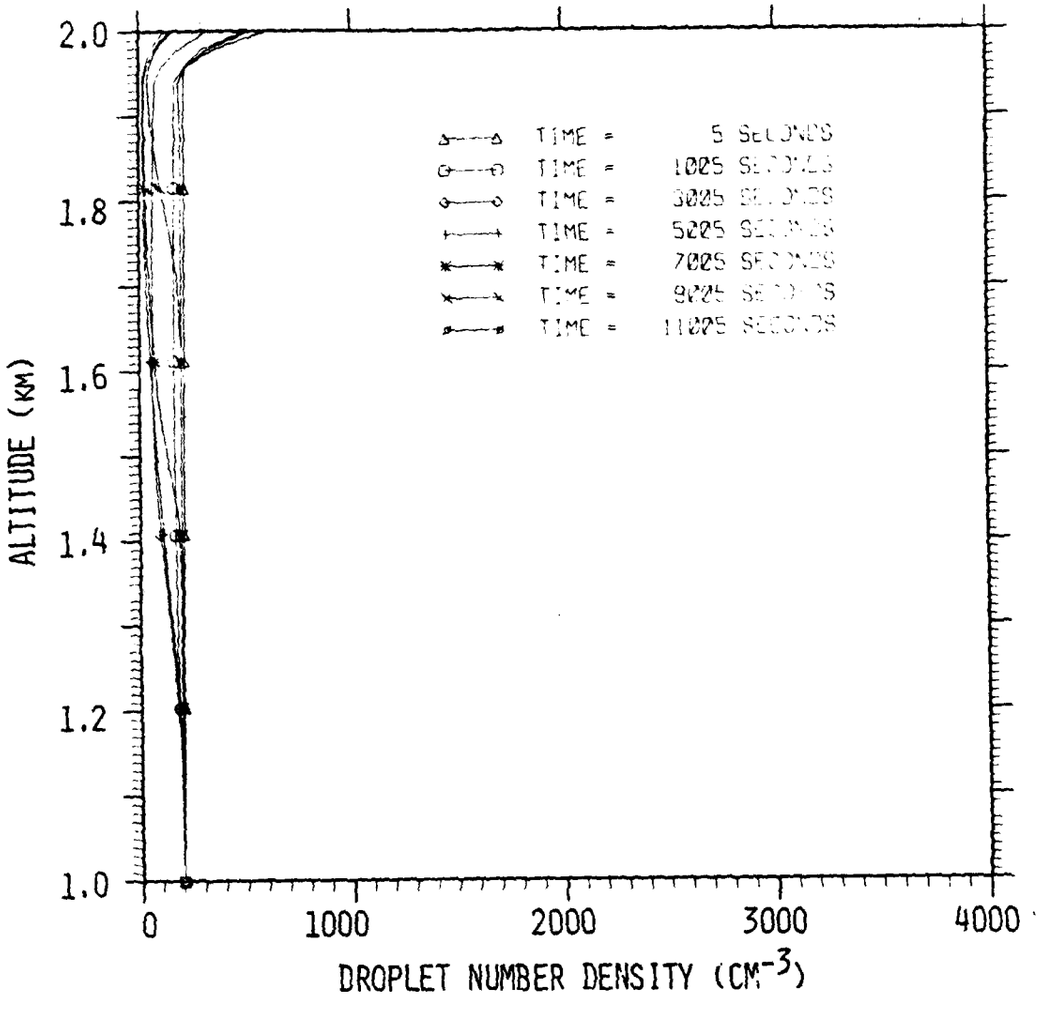

Fig. 4 - Droplet Number Density, Ice Particle Flux at Cloud Top is 1000 $m^{-2}s^{-1}$. Water Droplet Density at Cloud Bottom is 200 cm^{-3}

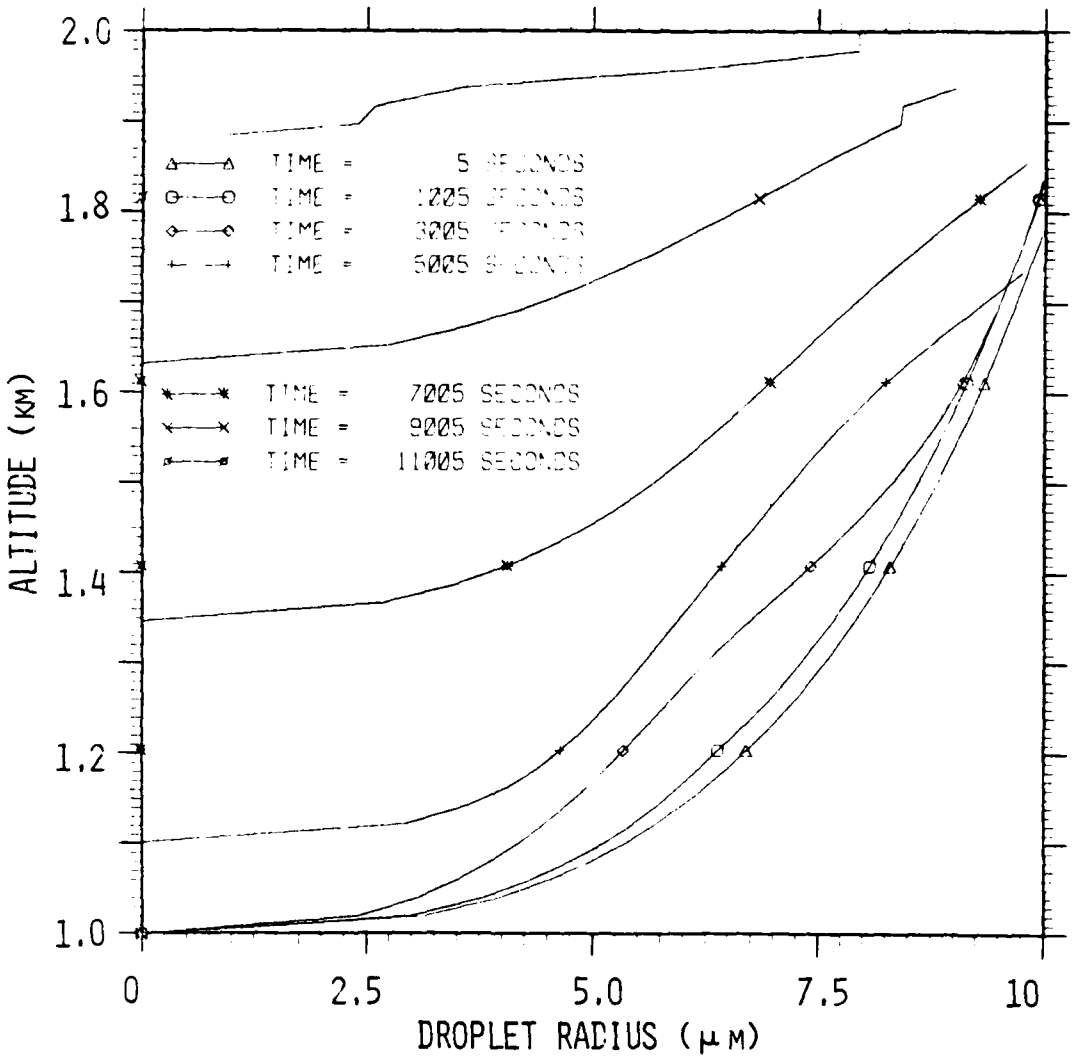

Fig. 5 - Droplet Radius. Ice Particle Flux at Cloud Top is 1000 $m^{-2}s^{-1}$. Water Droplet Density at Cloud Bottom is 200 cm^{-3}

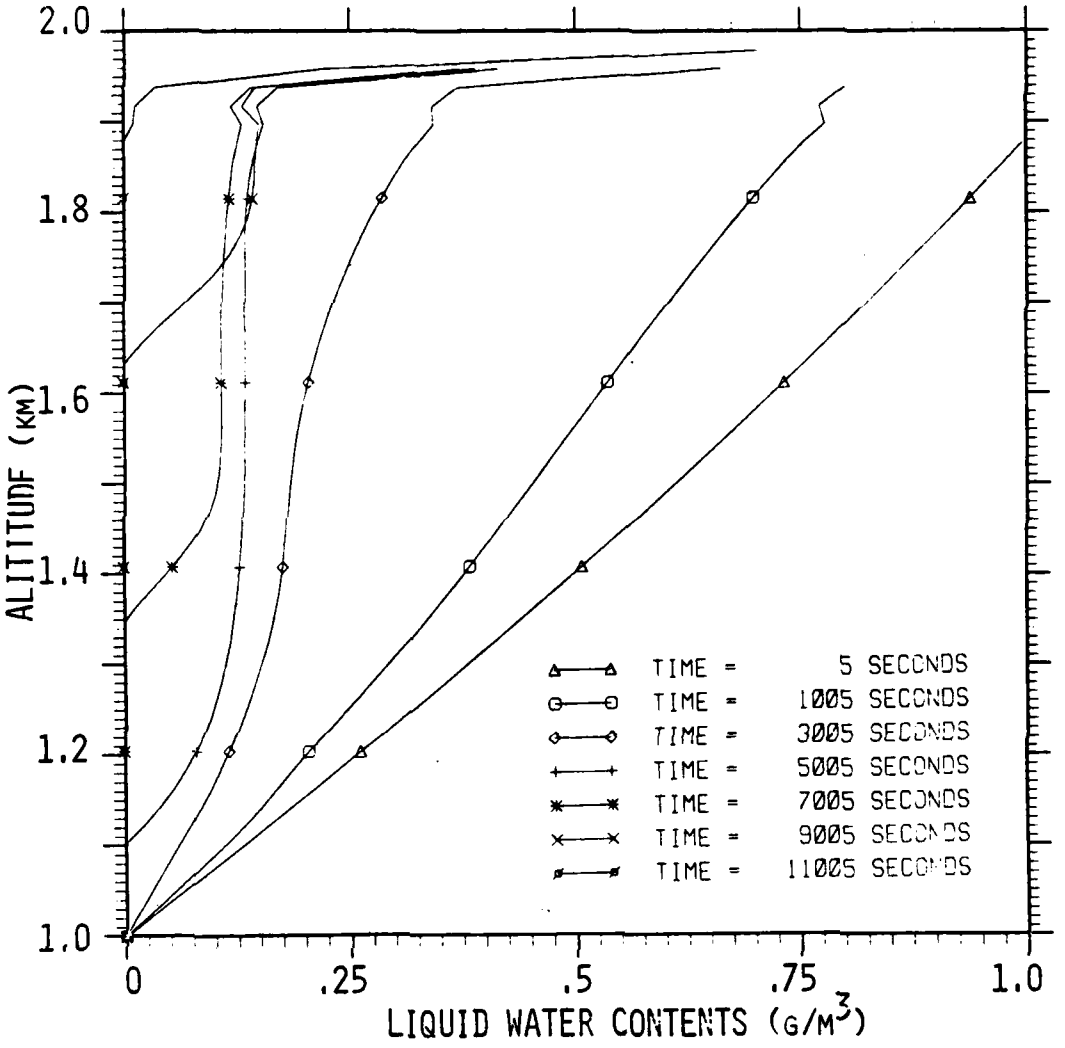

Fig. 6 - Liquid Water Content. Ice Particle Flux at Top is 1000 $m^{-2}s^{-1}$. Water Droplet Density at Cloud Bottom is 200 cm^{-3}

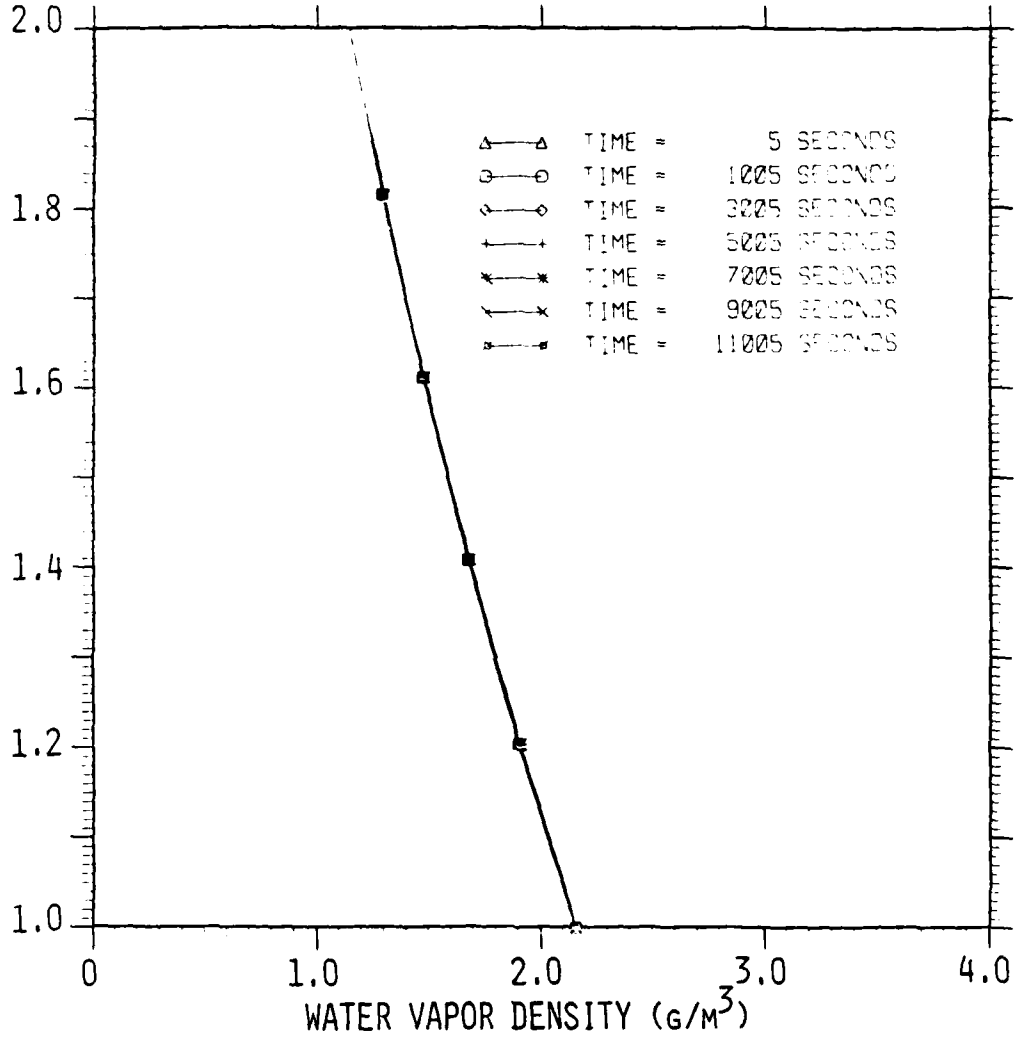

Fig. 7 - Water Vapor Density, Ice Particle Flux at Top is 1000 $m^{-2}s^{-1}$. Water Droplet Density at Cloud Bottom is 200 cm^{-3}

substantially greater ice accumulation at the cloud top, which would occur if slower growth happened there. This kind of accumulation is seen in the data of Ref. 10 for the mature and decaying stages; the authors of Ref. 10 attribute it to some sort of ice multiplication process. We believe it possible that large-scale accumulation may also result from slow growth, if conditions leading to cummulative vapor depletion are established. Continued work in improved modeling of the cloud top region is needed to clarify this point.

A pre-condition for glaciation is a sufficiently high ice particle concentration, or, conversely, a sufficiently low lapse rate, so that the ice phase may absorb all of the excess vapor carried by the updraft. Criteria for this threshold have been established, for example by Jiusto (Ref. 14); for our conditions it seems to correspond to about 3 particles/liter, as in the previous example.

To verify this limit, we repeated the calculations for similar conditions, except that the ice flux at the top was reduced by a factor of 2 (to 500 m^{-2} sec^{-1}). Figure 8 shows the development of the liquid water contents with time in their case; there is a strong reduction, traceable mostly to the continued accretion of droplets on ice particles, but the droplets show no tendency to evaporate in the presence of about 1 ice crystal/liter. Notice the ice concentration has decreased by a factor of 3, while the flux was reduced only by 2; this is due to the faster fall speed (0.8-1 m/sec vs 0.5-0.8 m/sec) of the particles in the second case, which in turn results from the continuation of riming throughout the cloud development. Figure 9 illustrates this; about half the mass per particle is rime, even after 11,000 sec. Also associated with this is the smaller radius of the ice particles (0.8 μm at cloud base), due to their smaller residence time. Altogether, then, the riming behavior of the ice particles cooperates

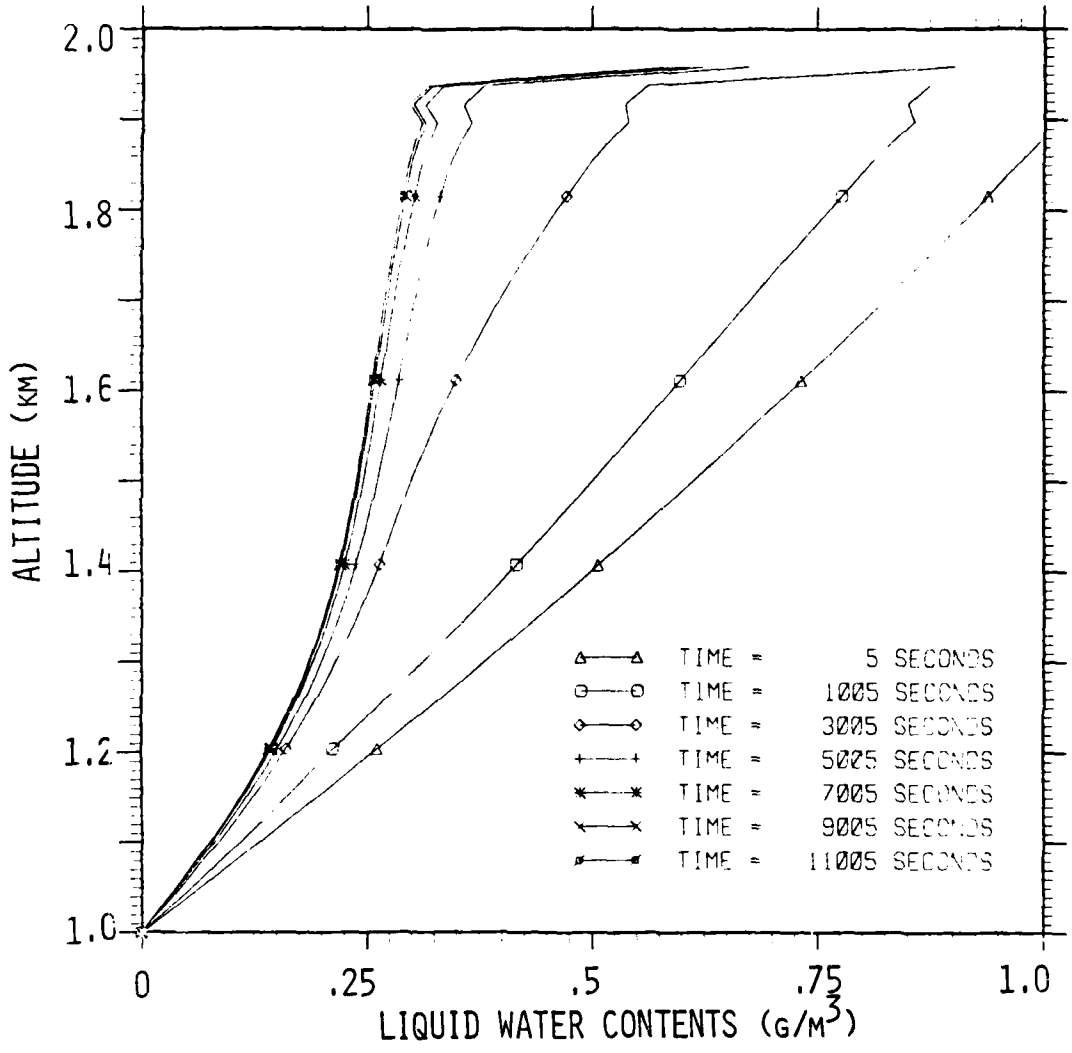

Fig. 8 - Liquid Water Content. Ice Particle Flux at Top is 500 $m^{-2}s^{-1}$. ater Droplet Density at Cloud Bottom is 200 cm^{-3}

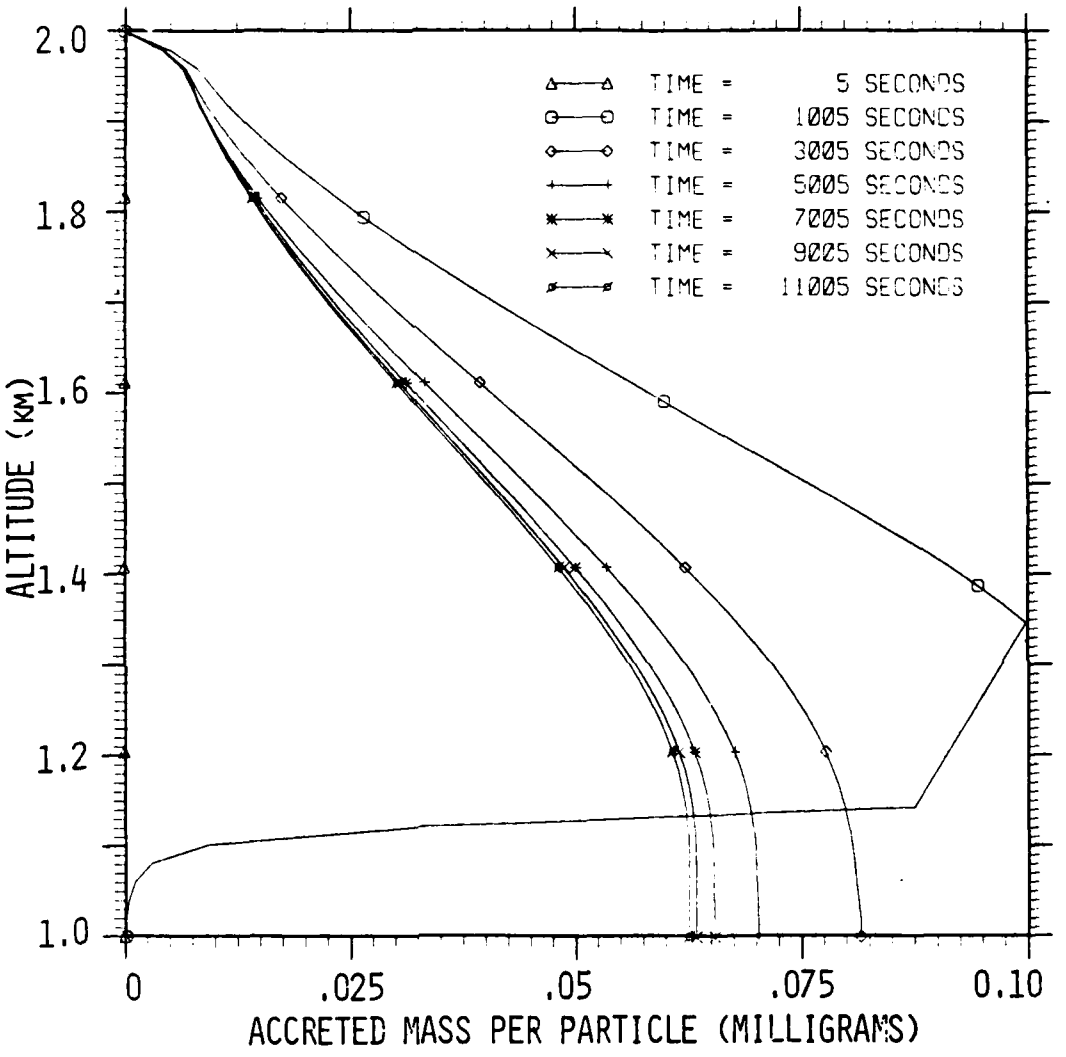

Fig. 9 - Accreted Mass per Particle. Ice Particle Flux at Top is 500 $m^{-2}s^{-1}$. Water Droplet Density at Cloud Bottom is 1000 cm^{-3}

in making a fairly fast transition from glaciating to non-glaciating conditions as the ice flux is reduced.

Going to the opposite end of the concentration scale, we tested a case with 2000 crystals/(m^2 sec) (twice the flux of the basic case). Simultaneously, the diameter of the droplets was reduced to about 12 μm, to reduce accretion effects. This resulted in a very rapid glaciation of the whole cloud between t = 3000 sec (when the, now lightly accreting crystals, first reach the cloud base) and about t = 4000 sec. The vapor density profiles for this case are shown in Fig. 10. The vapor is clearly below water saturation, but still only about half way to ice saturation. It would appear that in order to prevent vapor diffusion growth in the upper part of the cloud, a crystal seeding rate even two to three times higher is required; under such conditions, accumulation at the top can be expected.

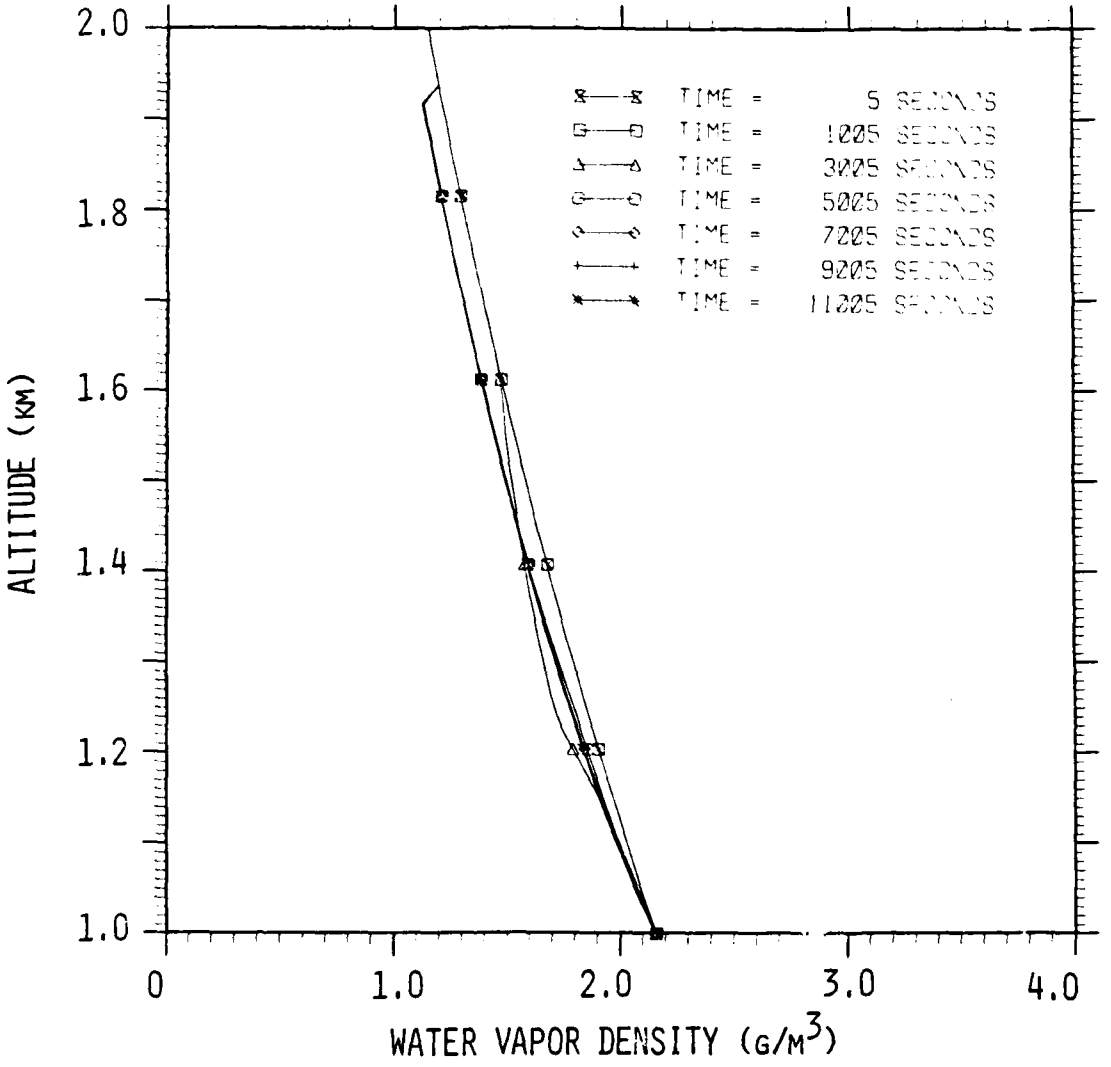

Fig. 10 - Water Vapor Density. Ice Particle Flux at Top is 2000 $m^{-2}s^{-1}$. Water Droplet Density at Cloud Bottom is 1000 cm^{-3}

5. OBSERVATIONS ON THE SNOW I DATA

Due to the apparent existence of agglomeration in at least parts of the snowstorms of January and February 1981, as reported in Ref. (11), we have not attempted a direct simulation using the numerical code. We will limit ourselves for now to a few comments on the implications of the data.

Figure 11 shows vertical profiles taken shortly after the start of snow on January 22. There is a nearly isothermal, relatively thin cloud which appears to be ice, rather than water saturated. Glaciation is, indeed, favored by low lapse rates, because a moderate ice particle concentration can then absorb the small amount of vapor made available by the updraft. However, the clouds may be reverting to liquid, since light to medium riming is reported later on the day. At the early times, the cloud could be classed as a "seeder-only" system, in the nomenclature of Jiusto and Weickmann (Ref. (15)).

Figure 12 corresponds to the peak of the snowstorm of February 8-9, 1981. The in-cloud temperature follows closely a moist adiabatic line, showing a well developed stratus system. The cloud is quite thick, water saturation being maintained to at least 3200m, with a low cloud base (~400m). The temperature range goes from -5°C to -25°C, which explains the wide variety of snow particles observed at the time. The very small columns reported may actually have formed near cloud base, in the -5 to -10°C range, while the more complex and large crystals must come from (or at least have gone through) the mid-regions of the cloud, around the maximum growth rate range (-12 to -18°C).

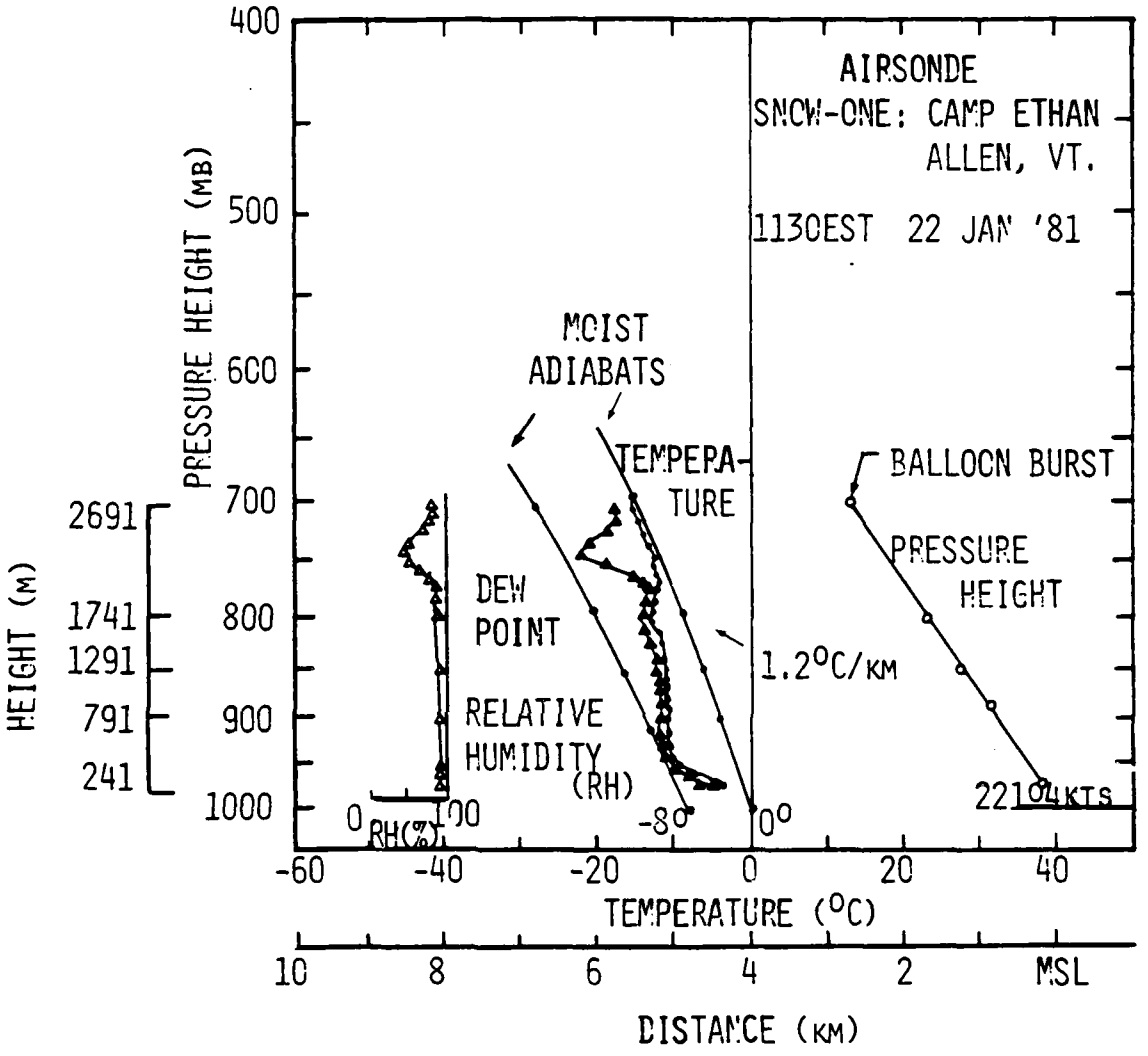

Fig. 11 - Data From Airsonde Flight, 1130, 22 January 1981 (From Reference (11), With Moist Adiabats Added)

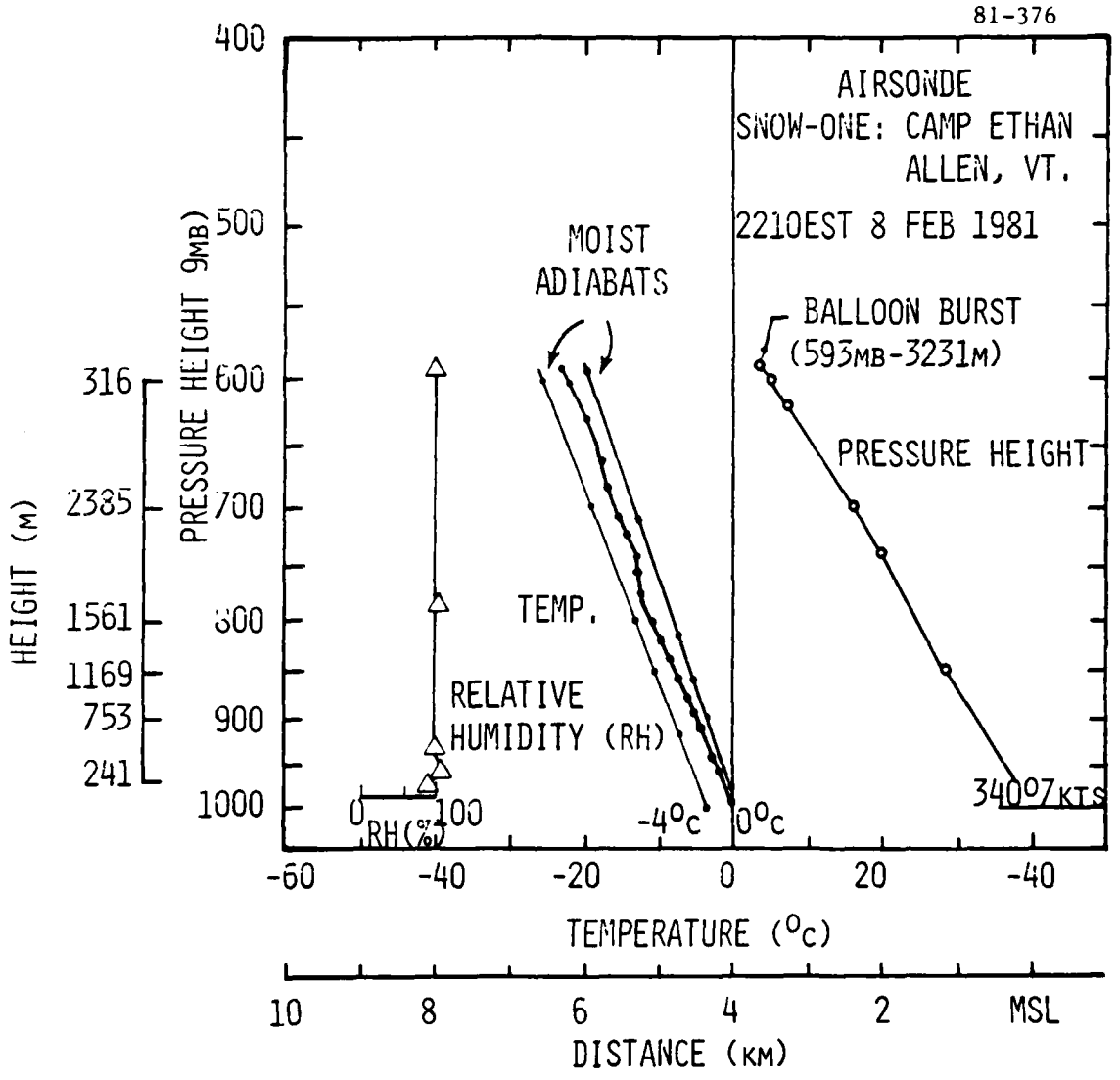

Fig. 12 - Data From Airsonde Flight, 2210, 8 February 1981 (From Reference (11), With Moist Adiabats Added)

The data of snow concentration and precipitation rate are shown in Fig. 13 plotted versus each other for comparison with the empirical correlation of Sekhon and Srivastava (Ref. (16)). Most points cluster about the correlation line, with corresponding fall velocities from 1 to 1.4 m/sec. For those points deviating clearly to the right (high fall velocities, 2-5 m/sec), one can recognize conditions of heavy riming in the descriptions reported.

It is of interest that Passarelli (Ref. (17)) has been able to obtain a theoretical prediction of the Sekhon-Srivastava line based on the existence of a limiting "equilibrium" growth regime, in which both agglomeration and vapor growth (with their opposite effects on polydispersity) are acting simultaneously. Based on the equations of Ref. (17) the equilibrium growth regime is only reached after a fall distance of the order of ℓ_{vp}/K_1, where ℓ_{vp} is the length scale for variation of vapor pressure in the cloud and K_1 is only a function of the exponents for the fall speed-diameter and vapor growth-diameter relationships; typical values of K_1 are about 0.3. Using the Clausius-Clapeyron equation, then, we obtain a "development distance"

$$\ell \simeq \frac{1}{0.3} \frac{R_v^2 T}{\Gamma L} \tag{19}$$

where R_v is the vapor gas contant, L_s the heat of sublimation and Γ the lapse rate. For $T = -16°C$, $\Gamma = 7°C/Km$, one finds $\ell \simeq 5000m$. Thus, only for rather thick strata can one expect strict equilibrium growth, although a good approximation seems to be obtained in only a fraction of the above distance. In any event, Fig. 13 seems to confirm the importance of agglomeration for the case of the February 8-9 storm.

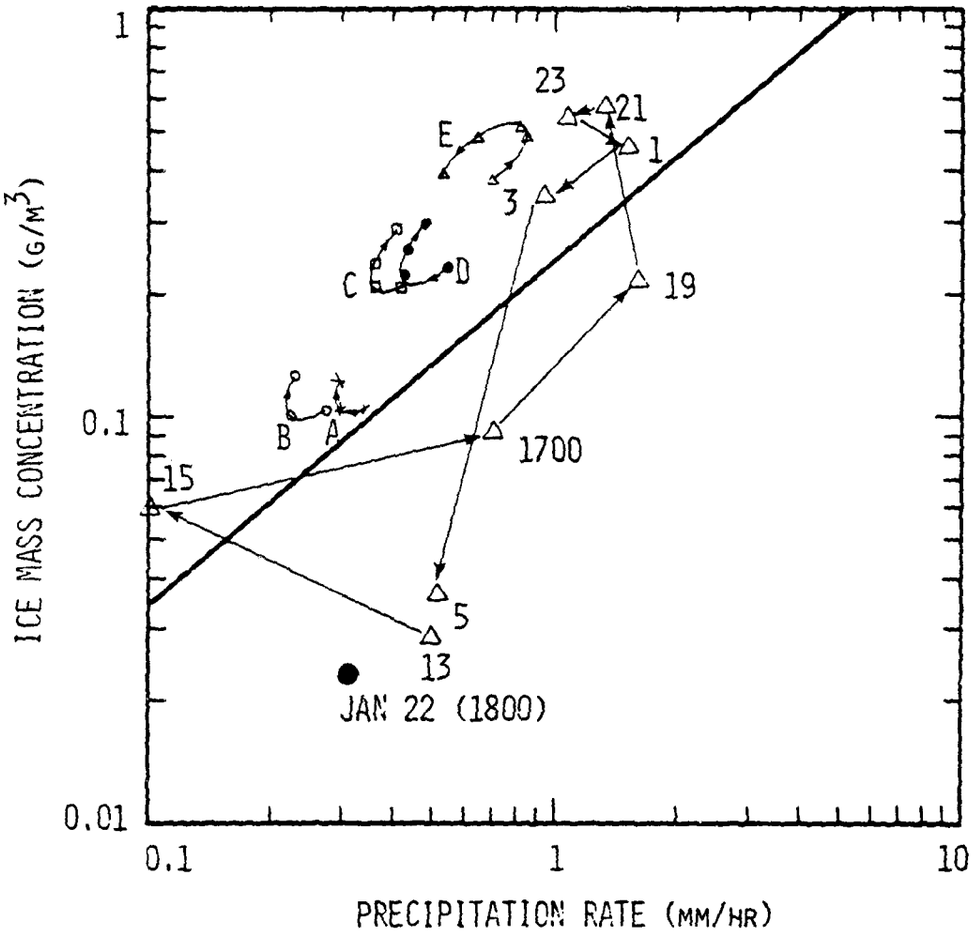

Fig. 13 - Triangles are Feb. 8-9, 1981 Storm Data (Time of Day Indicated) Solid Dot is From Jan. 22, 1981 Storm The Solid Line is Sekhon-Srivastava Correlation (Ref. 16) Dotted Lines are Model Results

(A) Case 500/2/8 (B) Case 500/5/8 (C) Case 1000/2/8
(D) Case 1000/1/8 (E) Case 2000/10/8

Also shown in Fig. 13 are the results of our model calculations at cloud base, for five sets of conditions. These are denoted by the code a/b/c, where a is the crystal flux (per m^2, per sec), b is 10^{-8} x the droplet density at cloud base (m^{-3}), and c is the lapse rate in the upper 400m of the cloud, in °C/km (the lower 600m are in all cases taken at 8°C/km). The trends predicted are correct, but our calculated fall velocities tend to be lower than observed in the SNOW data and than implied by the correlation data. This is most likely a result of the neglect of agglomeration, which increases particle mass somewhat faster than exposed area.

6. SNOW OPTICS TRANSMITTANCE CALCULATIONS

In this section we develop a relationship between extinction coefficients in the visible/infrared to snowflake physical characteristics. We begin with the equation for the transmission τ through falling snow

$$\tau = \exp(-\beta L) \quad , \tag{20}$$

where

L = path length

β = extinction coefficient = $\int_A N(A) Q_{ext}(n_{ice}, A, \lambda)\, dA$

$N(A)$ = number of snowflakes with area A

Q_{ext} = extinction efficiency

n_{ice} = refractive index of ice

λ = wavelength

The equation for conservation of mass gives

$$M_{water} = M_{ice} \quad ,$$

where

M_{water} = melted-ice water equivalent of snow

M_{ice} = mass of ice

$$\rho_{water} R = \rho_{ice} \int VN(V)v(V)\, dV \tag{21}$$

ρ_{water} = density of water

R = precipitation rate

ρ_{ice} = density of ice

$N(V)$ = number of snowflakes with volume V

$v(V)$ = settling velocity of snowflake with volume V .

Dividing Eq. (21) by Eq. (20) and solving for β:

$$\beta = \frac{\rho_{water} R \int AN\, Q_{ext}\, dA}{\rho_{ice} \int VN\, v\, dV} \tag{22}$$

For a monodisperse particle distribution, $N(V) = N_o\delta(V-V_o)$ and $N(A) = N_o\delta(A-A_o)$, in which case Eq. (22) becomes:

$$\beta = \frac{\rho_{water} R}{\rho_{ice}} \frac{A_o Q_{ext}}{V_o v} \tag{23}$$

For visible/infrared, $Q_{ext} = 2$, so that a relatively simple formula for β results:

$$\beta = \frac{2\rho_{water} R}{\rho_{ice}} \left(\frac{A_o}{V_o v} \right) \qquad (24)$$

Data exists (e.g., Refs. 2,18,19) on values of β, A, V, and v for different snow types. The data points shown in Figures 14 and 15 were digitized for subsequent curve fitting. (The original curves shown in Figure 14 and 15 are drawn with unknown curve fits.)

Appendix A shows the curve fit results for fall velocity v versus dimension for different snow crystal type. Appendix B gives the results for mass M (actually the 3/2 power of the linear dimension designated "r" in Figure 15).

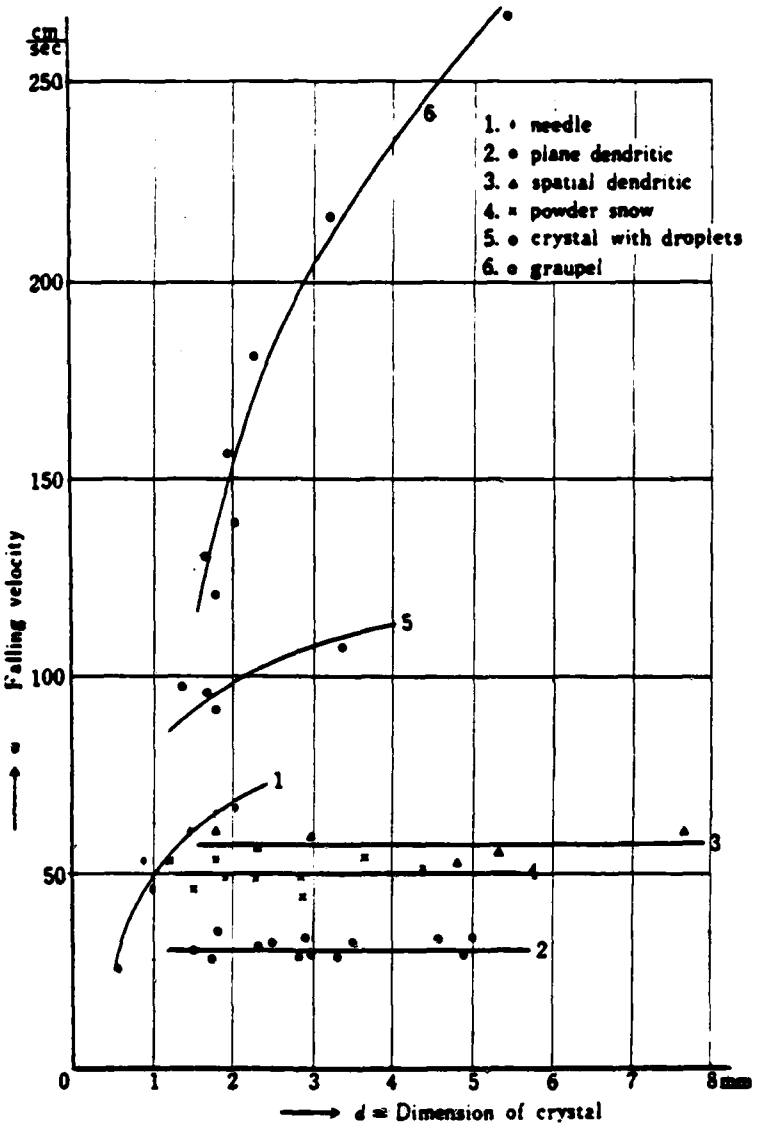

Fig.14 - Snowflake Fall Velocity Data Versus Dimension for Different Snow Crystals. Original Data with Unknown Curve Fits (Ref.2).

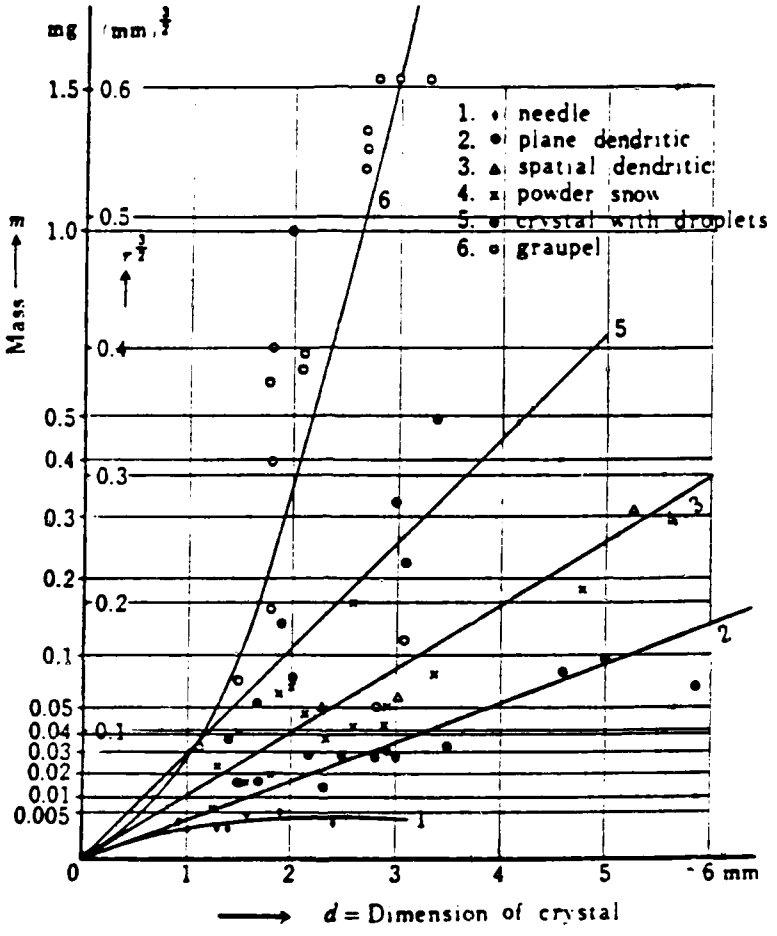

Fig.15 - Snowflake Mass Versus Dimension. Original Data With Unknown Curve Fits (Ref. 2)

7. CONCLUSIONS AND RECOMMENDATIONS

A relatively simple model has been developed that can be used for exploration of the intricate sensitivities and interrelationships affecting the nature and intensity of snowfall. Although the model can be of use in its present form, preliminary evaluations against data indicate the need for several improvements and extensions.

(a) Inclusion of ice-ice agglomeration

(b) Elimination of fictitious accumulations due to updraft dropoff.

(c) Inclusion of wet snow effects

The work has also led to the awareness that more detailed in-cloud measurements would greatly enhance our understanding and predictive capabilities. Models like the present one could be used to evaluate and correlate these detailed data.

Finally, a simple relationship between extinction in the visible/infrared and snowflake physical characteristics provides a framework in which the snowflakes resulting from calculations performed by the model described above can be related to optical transmission data.

8. REFERENCES

1. Ebersole, J.F., Caulfield, H.J. and Spaulding, T.E., Part 1 of "Modeling the Dynamics and Optical Effects of Snowstorms," and M. Martinez-Sanchez, D.S. Dvore, and R. Vaglio-Laurin (Part II) ," Aerodyne Research, Inc., (Snow Symposium Meeting, August 1981).

2. Nakaya, U., "Snow Crystals Natural and Artificial," Harvard University Press, Cambridge, MA (1954).

3. Magono, C. and Lee, C.W., "Meteorological Classification of Natural Snow Crystals," J. of Faculty of Science, Hokkaido University, Japan, Ser. VII, Vol. II, No. 4, p. 321 (1966).

4. Ryan, B.F., J. de Mech. Atmos. Vol. 6, p. 673 (1972).

5. Pitten, R.L., J. Atmos. Sci. Vol. 34, p. 684 (1977).

6. Schlamp, R.J., Pruppacher, H.R., and Hamielec, A.E., 1975, J. Atm. Sci. Vol. 32, p. 2330.

7. Davis, C.I., Ph.D. Thesis, Dept. Environ. Sci., University of Wyoming, Laramie, Wyoming (1974).

8. Heymsfield, A., J. Atmos. Sci. 29, 1348 (1972).

9. Young, Kenneth C., "A Numerical Simulation of Wintertime, Orographic Precipitation: Part I. Description of Model Microphysics and Numerical Techniques," J. Atm. Sci. Vol. 31, p. 1735 (October 1974).

10. Magono, C. and Lee, C.W., J. Meteor. Soc. Japan 51, 176, (1973).

11. Preliminary Snow One Data Report, April 1981, CRREL, Hanover.

12. Pruppacher, H.R. and Klett, J.D., Microphysics of Clouds and Precipitation (1978).

13. Squires, P. and Turner, J.S., 1962. Tellus, Vol. 4, p. 422.

14. Jiusto, J.E., Snow Crystal Development in Supercooled Clouds, Proc. 1st Nat. Conf. on Weather Mod., Albany, AMS, 287-295 (1968).

15. Jiusto, J.E., "Types of Snowfall," Bulletin American Meteorological Society, Vol. 54, No. 11, p. 1148 (November 1971).

16. Sekhon, R.S. and Srivastava, R.C., 1970, "Snow Size Spectra and Radar Reflectivity," J.Atmos. Sci., Vol./27, pp. 299-307.

17. Passarelli, R.E., Jr., "An Approximate Analytical Model of Vapor Deposition and Aggregation Growth of Snowflakes," J.Atm. Sci., Vol. 34, p. 118 (1978).

18. J.B. Mason, "Light Attenuation in Falling Snow," ASL Technical Report ASL-TR-0013 (1978).

19. H.W. O'Brien, "Visibility and Light Attenuation in Falling Snow," J. Appl. Meteorology, Vol. 9, p. 671 (1970)

APPENDIX A

DIMENSION OF CRYSTAL

VS.

FALLING VELOCITY

FOR SIX TYPES OF SNOW

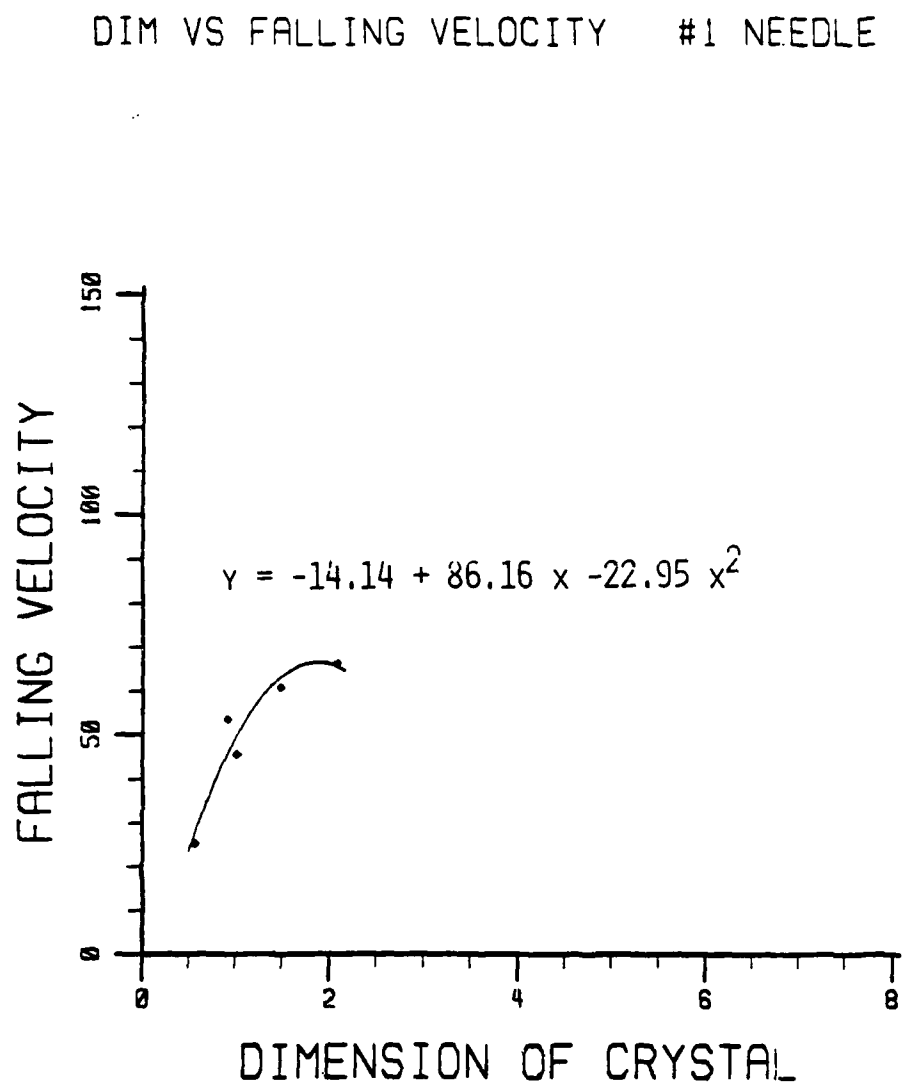

Figure A-1. Crystal dimension (mm) vs falling velocity (cm/s) for needles.

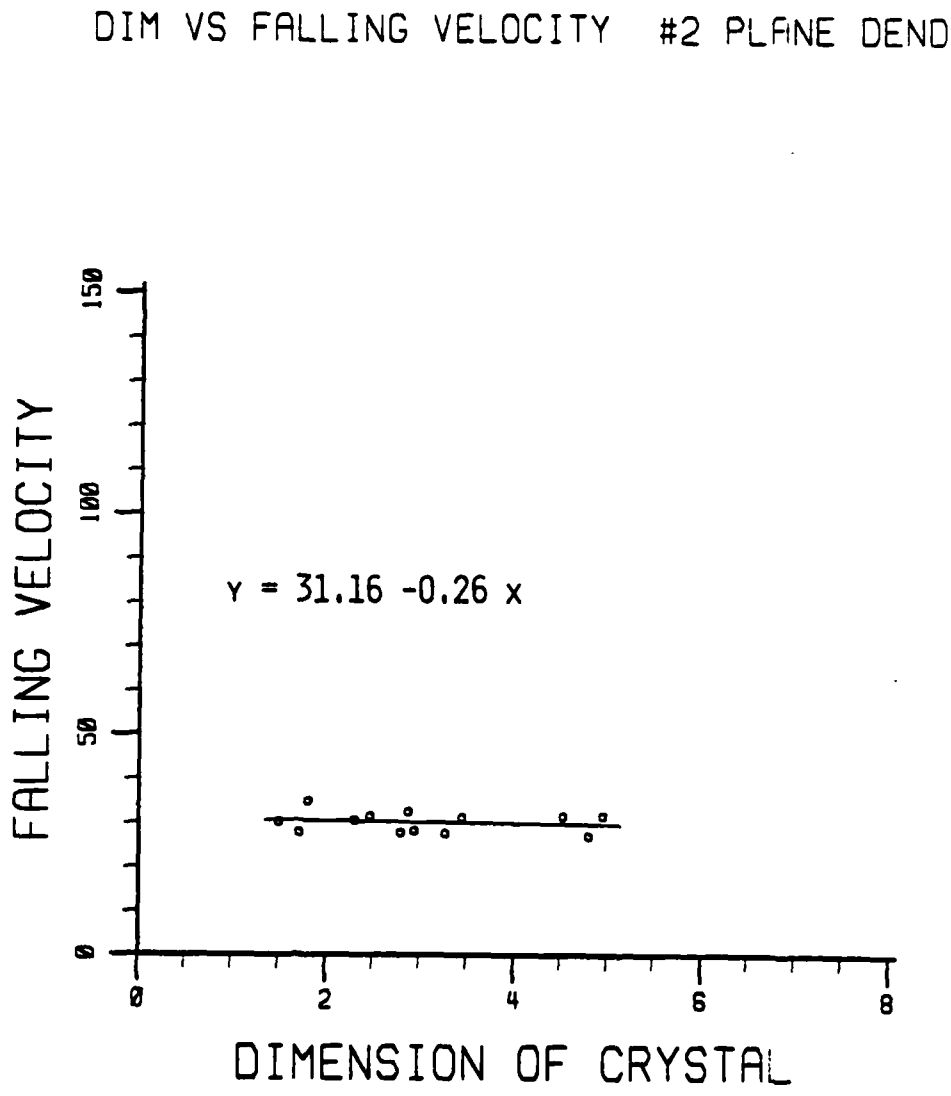

Figure A-2. Crystal dimension (mm) vs falling velocity (cm/s) for plane dendritic.

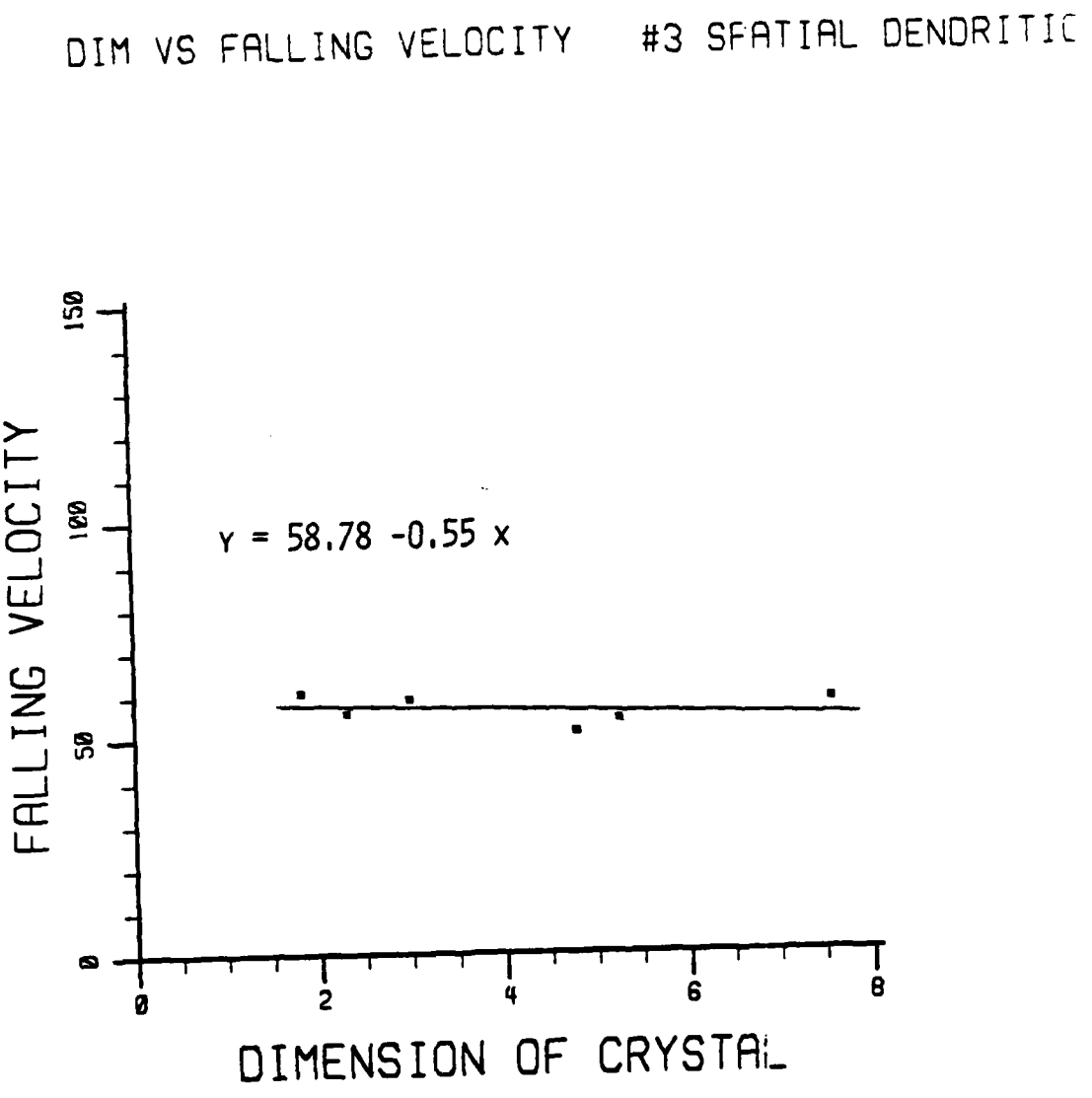

Figure A-3. Crystal dimension (mm) vs falling velocity (cm/s) for spatial dendritic.

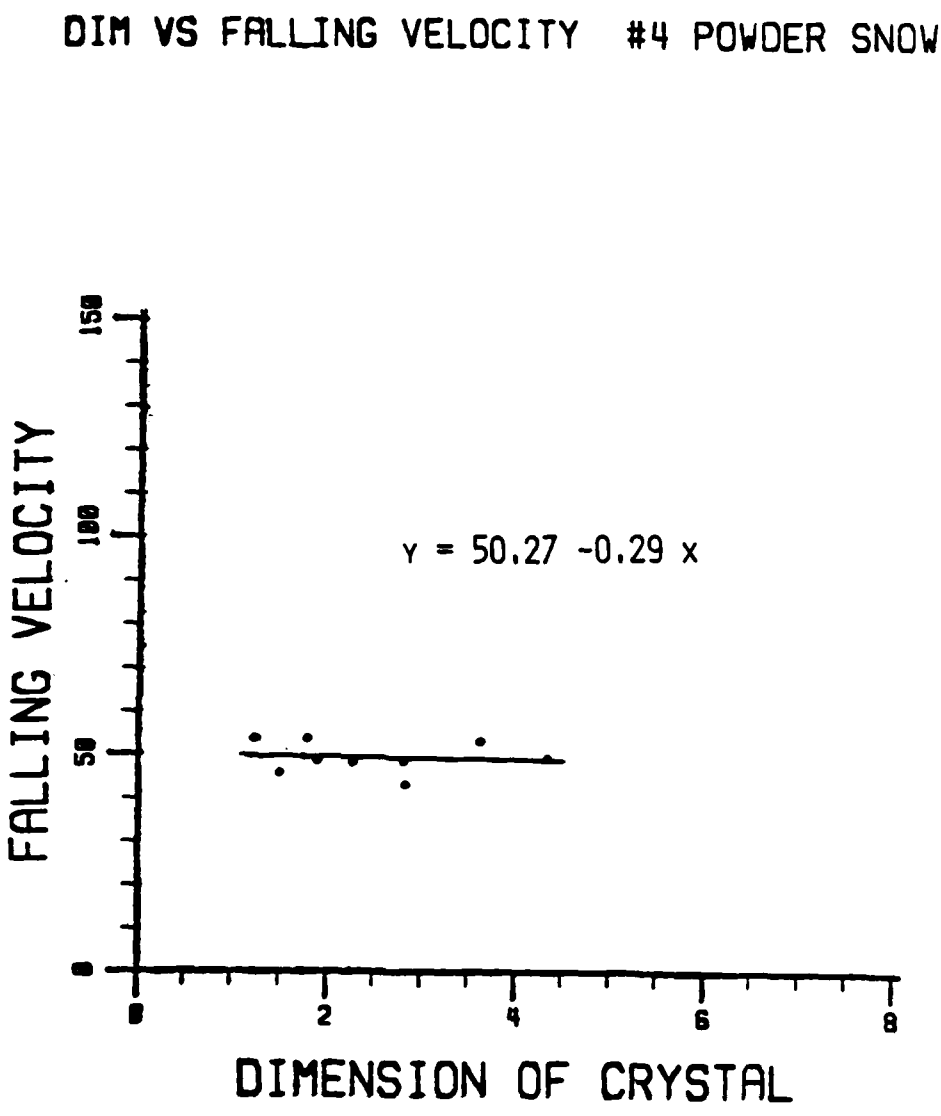

Figure A-4. Crystal dimension (mm) vs falling velocity (cm/s) for powder snow.

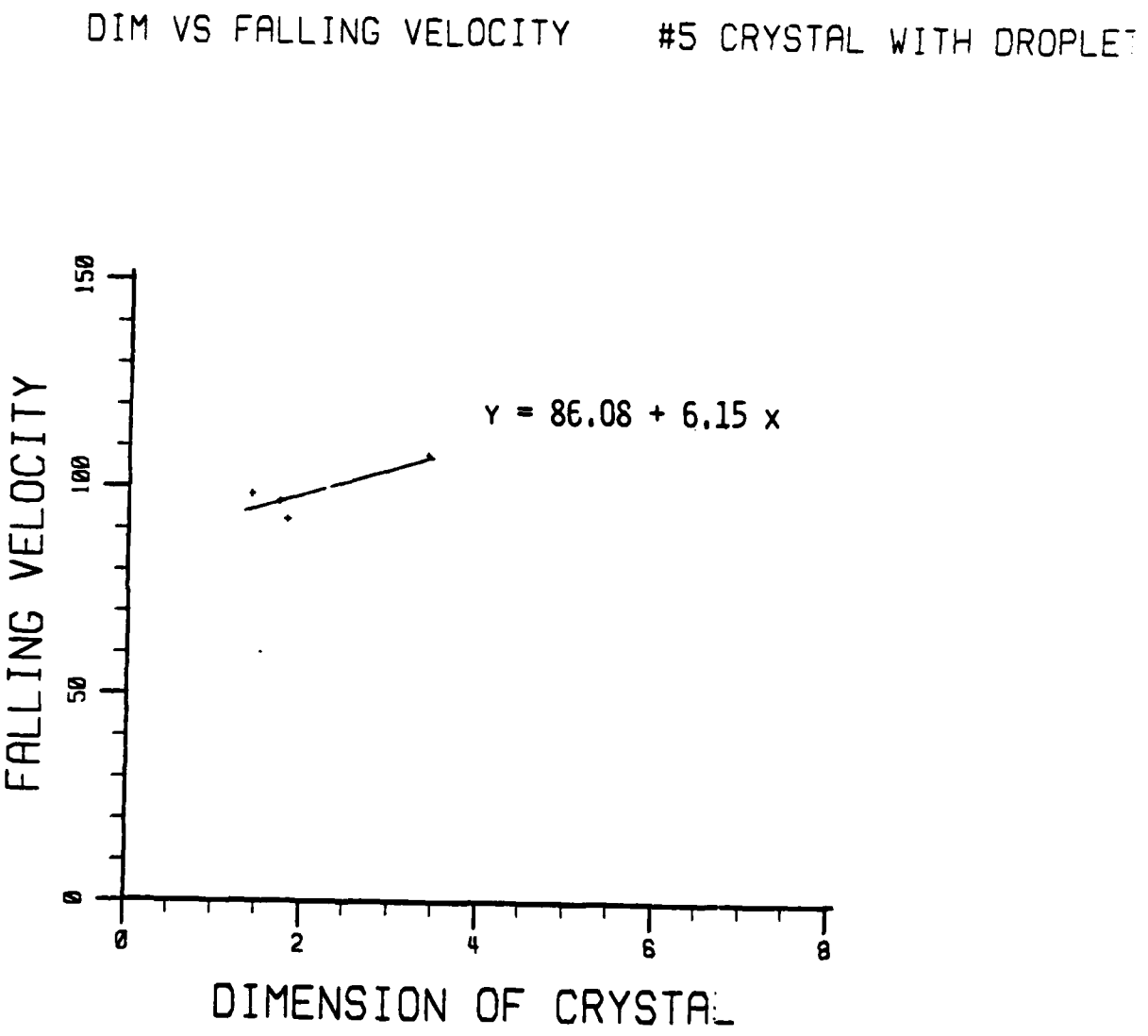

Figure A-5. Crystal dimension (mm) vs falling velocity (cm/s) for crystal with droplet.

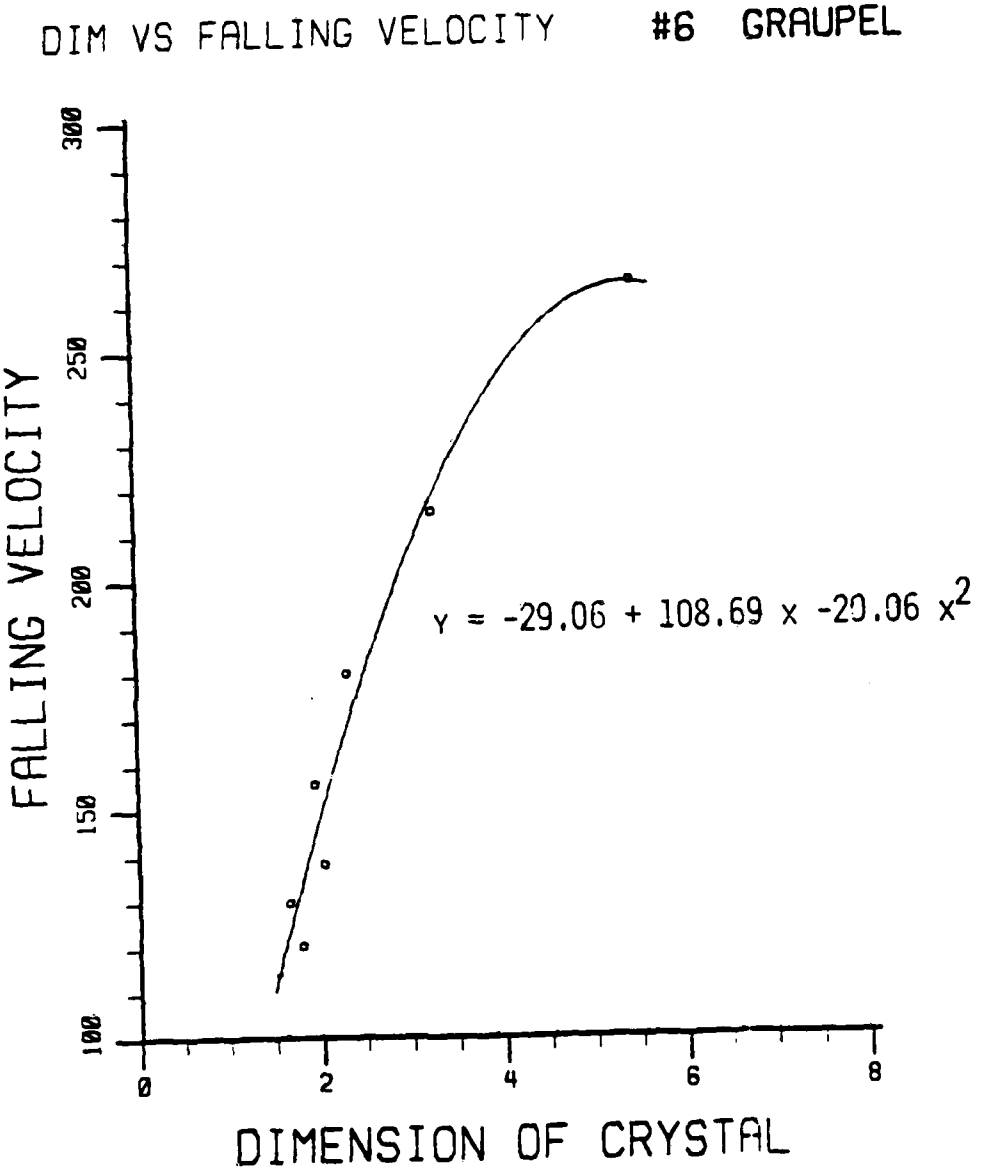

Figure A-6. Crystal dimension (mm) vs falling velocity (cm/s) for graupel.

APPENDIX B

DIMENSION OF CRYSTAL

VS.

R** (3/2)

FOR SIX TYPES OF SNOW

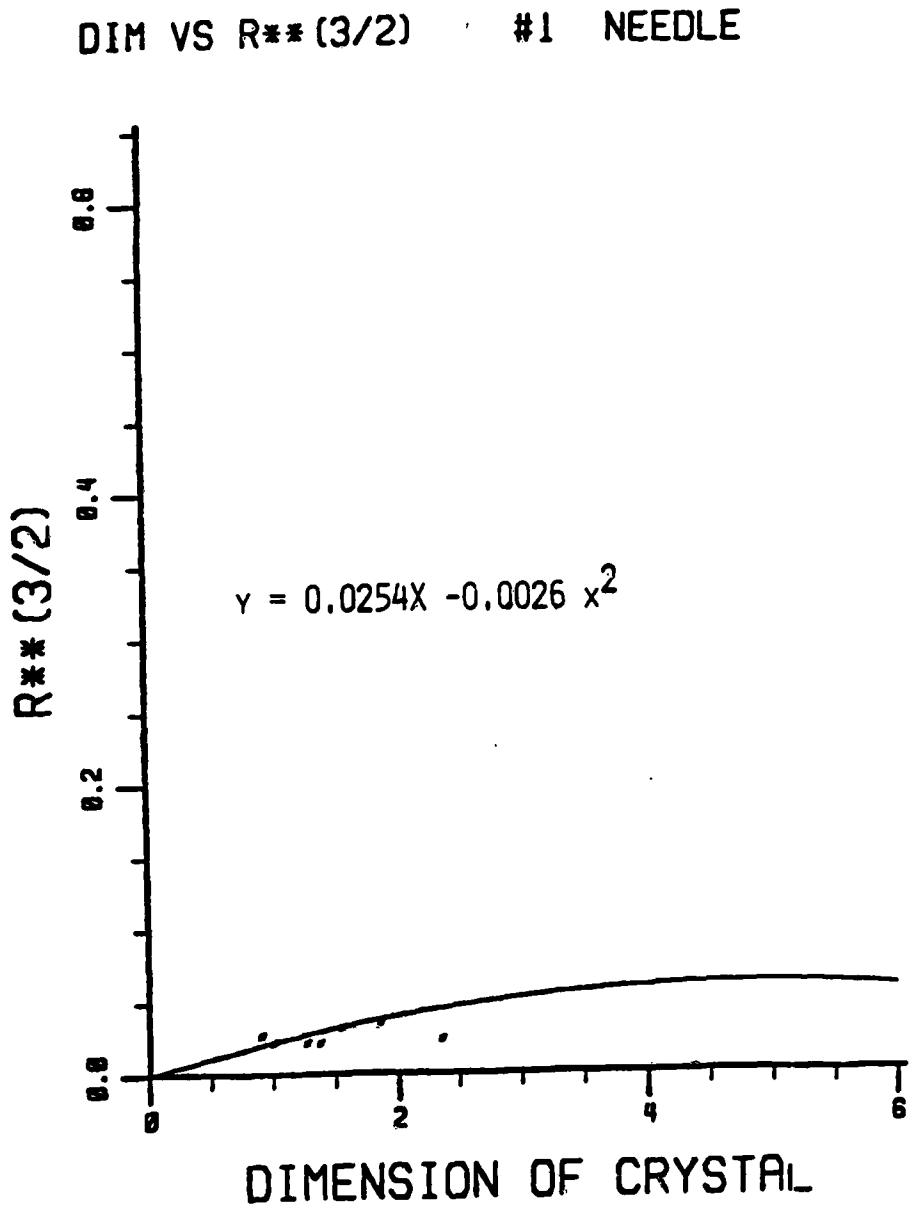

Figure B-1. Crystal dimension (mm) vs r (mm) to the 3/2 power for needles.

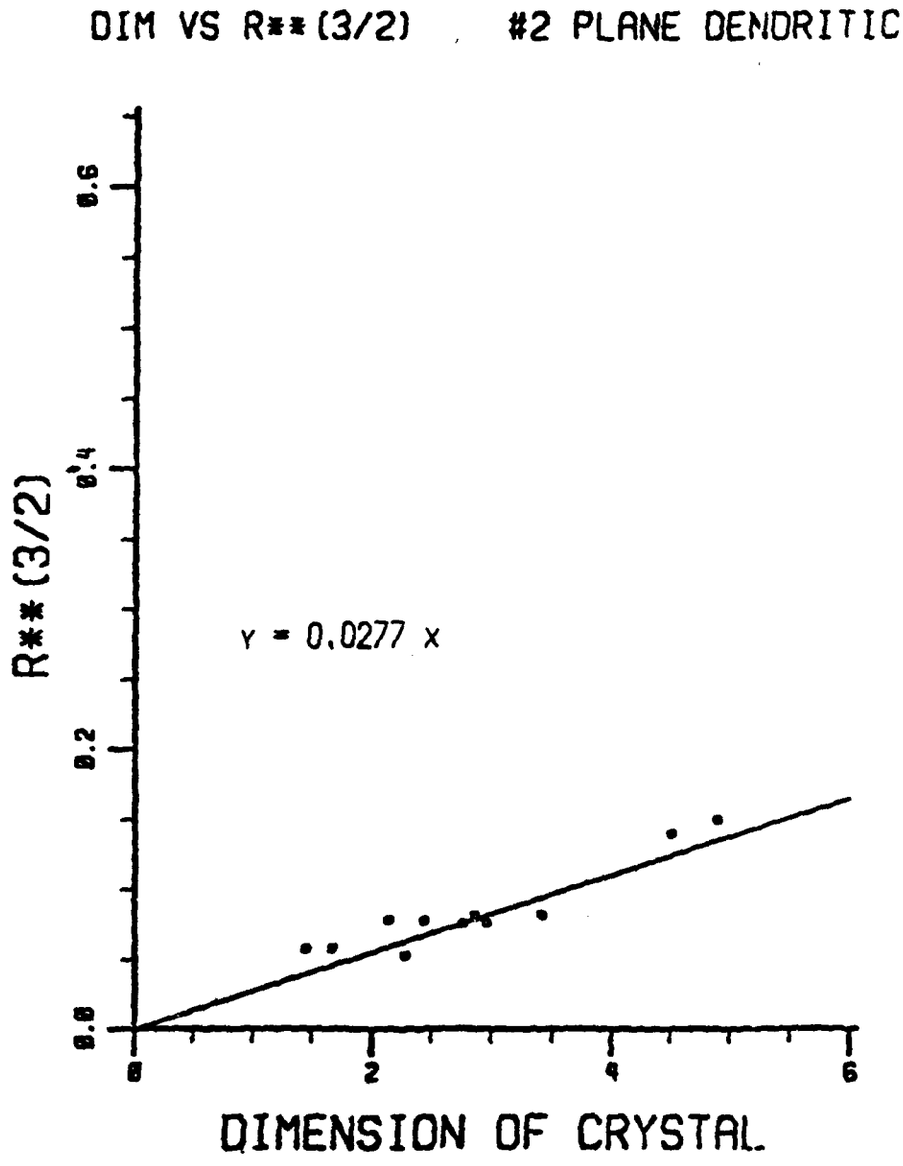

Figure B-2. Crystal dimension (mm) vs r (mm) to the 3/2 power for plane dendritic.

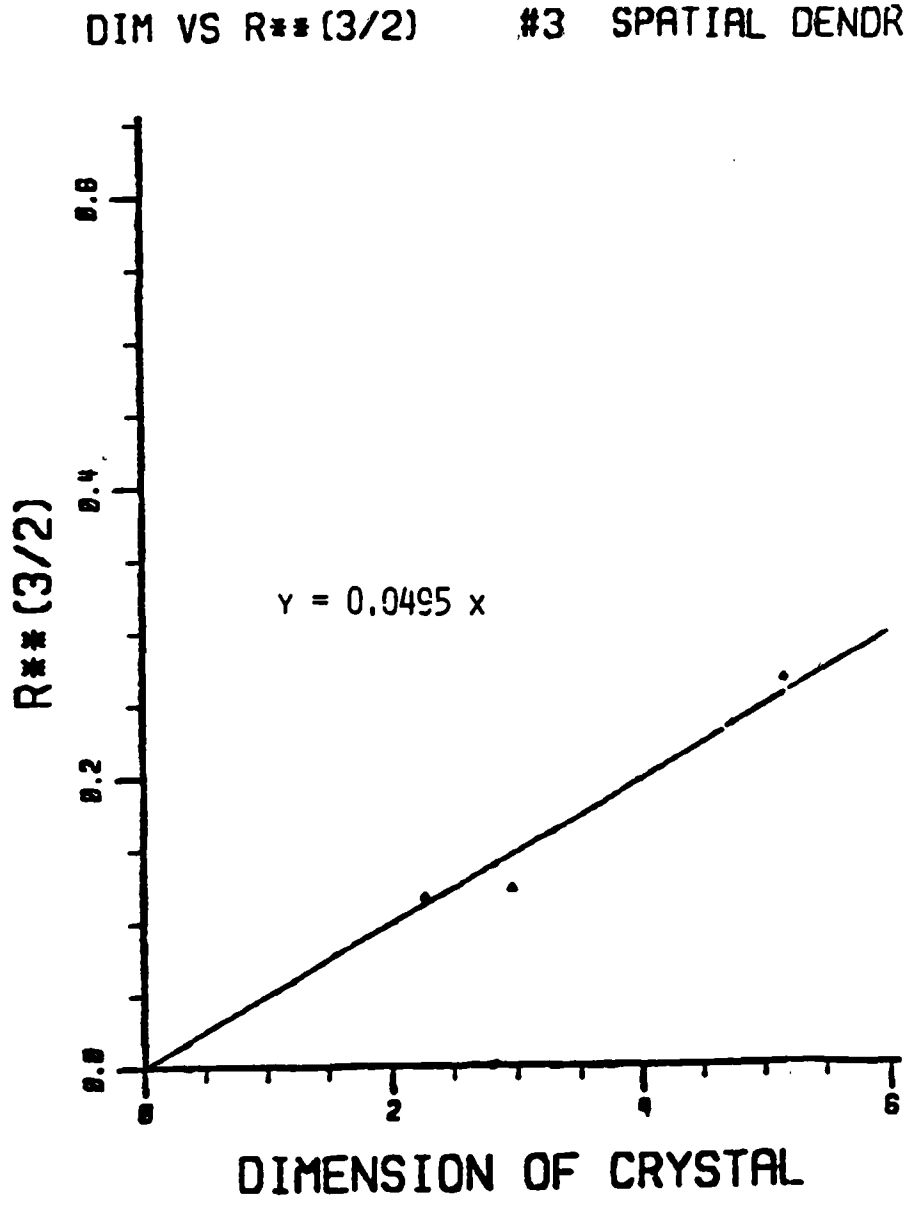

Figure B-3. Crystal dimension (mm) vs r (mm) to the 3/2 power for spatial dendritic.

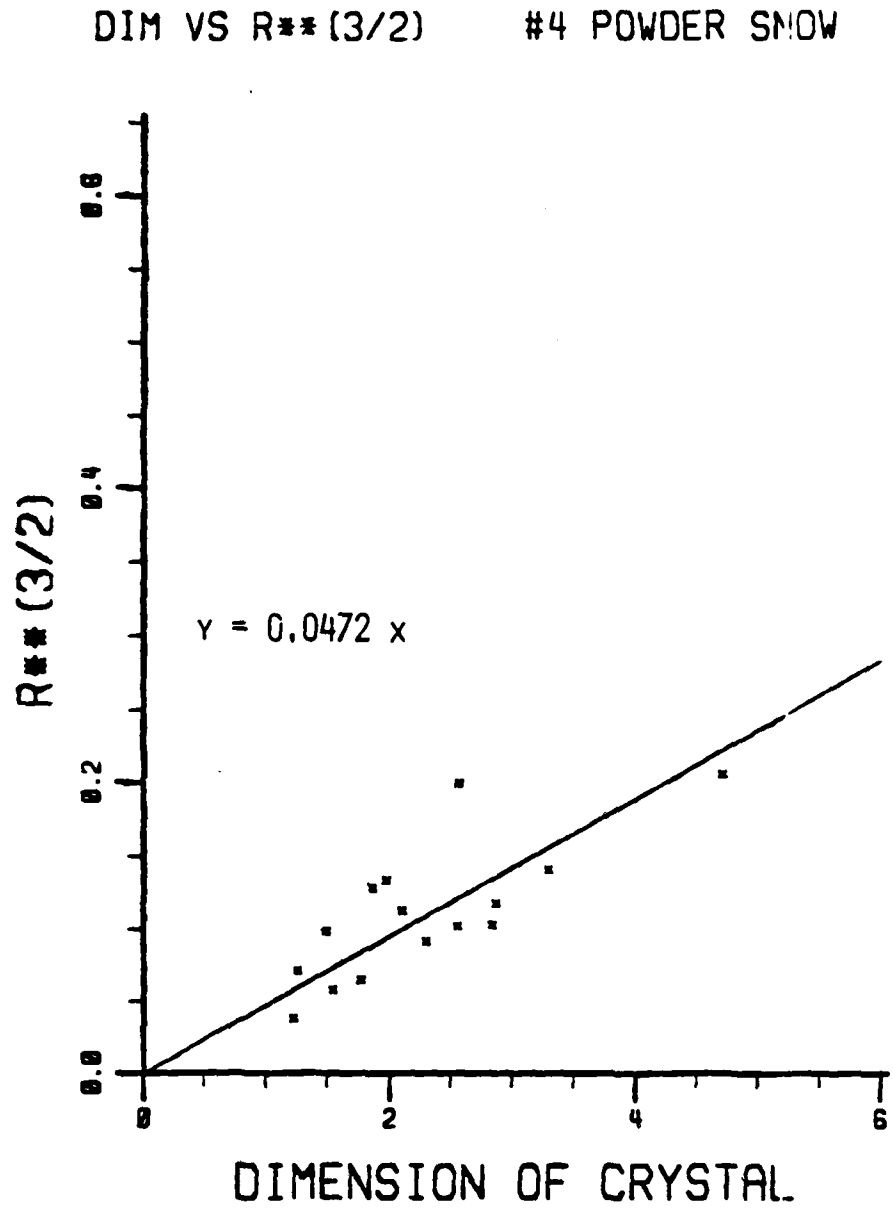

Figure B-4. Crystal dimension (mm) vs r (mm) to the 3/2 power for powder snow.

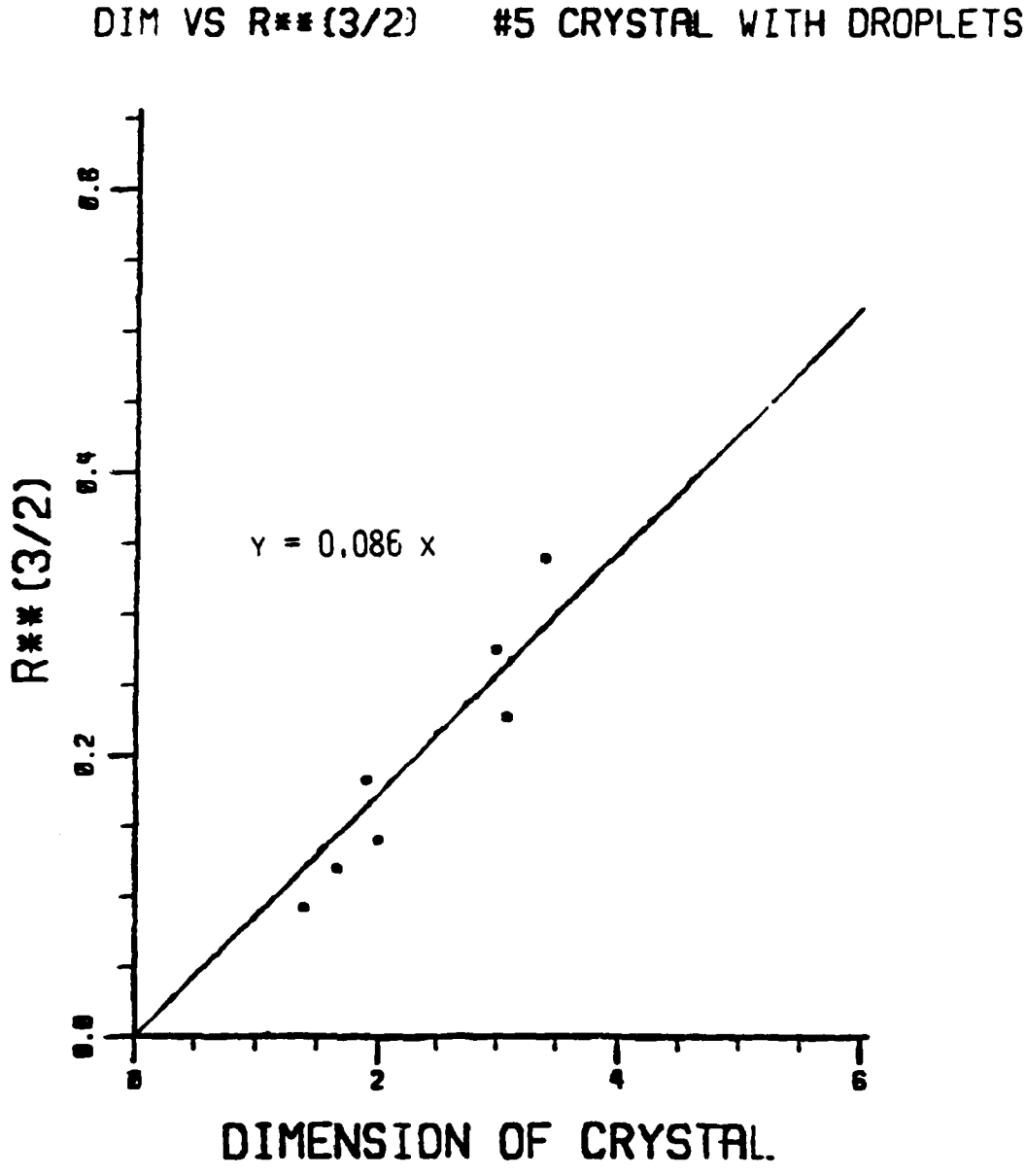

Figure B-5. Crystal dimension (mm) vs r (mm) to the 3/2 power for crystal with droplet.

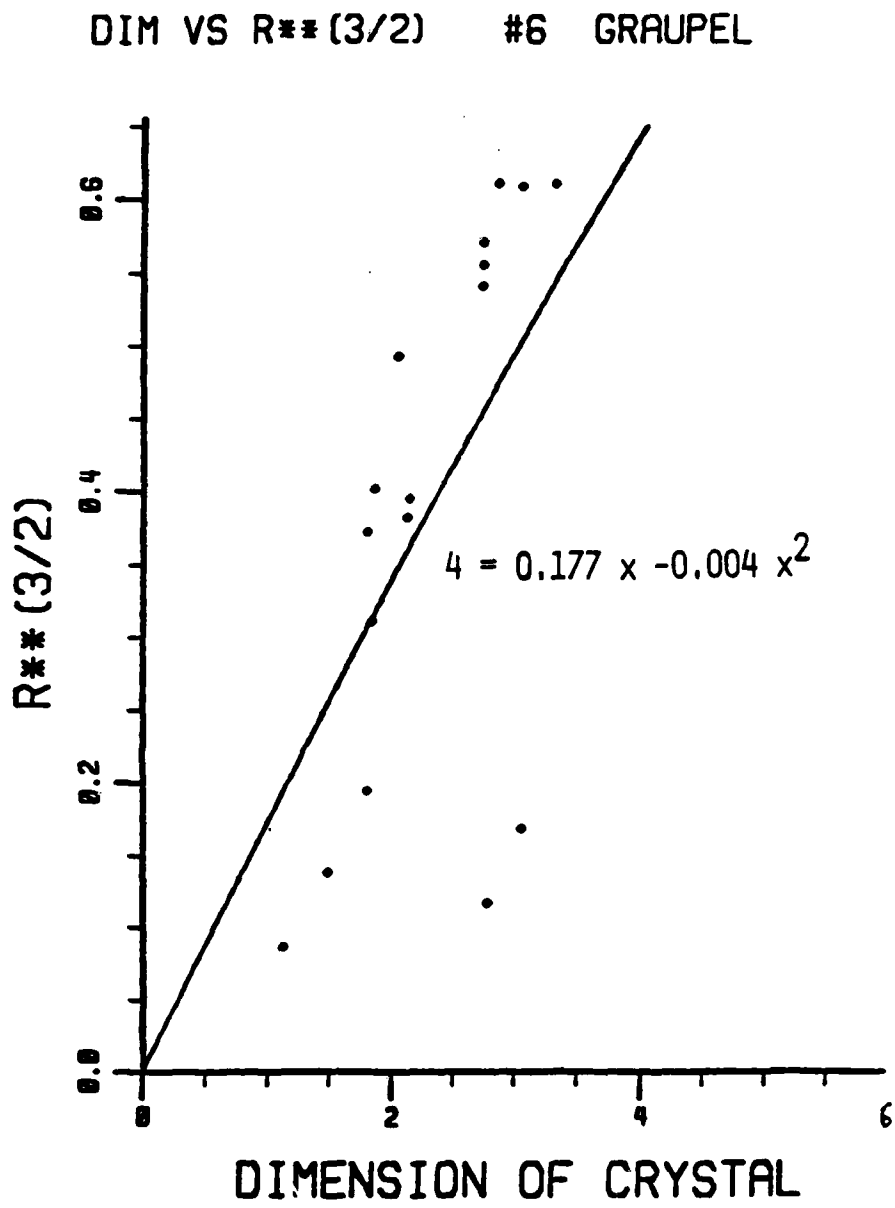

Figure B-6. Crystal dimension (mm) vs r (mm) to the 3/2 power for graupel.


DAT
FILM